J. Fluid Mech. (1994), *vol.* 276, *pp.* 21–59

The effect of phase variations and cross-shear on vortical structures in a plane mixing layer

By KRIS J. NYGAARD[1] AND ARI GLEZER[2]

[1] Exxon Production Research Company, PO Box 2189, Houston, TX 77252, USA

[2] Woodruff School of Mechanical Engineering, Georgia Institute of Technology, Atlanta, GA 30332-0405, USA

(Received 18 November 1992 and in revised form 10 January 1994)

The evolution of spanwise phase variations of nominally two-dimensional instability modes in a plane shear layer is studied in a closed-return water facility using time-harmonic excitation having spanwise-non-uniform phase or frequency distributions. The excitation waveform is synthesized by a linear array of 32 surface film heaters flush-mounted on the flow partition. A spanwise-linear phase distribution leads to the excitation of oblique waves and to the rollup of oblique primary vortices. When the prescribed phase distribution is piecewise-constant and spanwise-periodic, the flow is excited with a linear combination of a two-dimensional wavetrain and pairs of equal and opposite oblique waves, the amplitudes of which depend on the magnitude of the phase variation $\Delta\Phi$. As a result of the excitation, the primary vortices undergo spanwise-non-uniform rollup and develop spanwise-periodic deformations that induce cross-shear and secondary vortices in the braid region. The amplitude of the deformations of the primary vortices and the shape and strength of the secondary vortices depend on the magnitude of $\Delta\Phi$. When $\Delta\Phi$ is small, the secondary vortices are counter-rotating vortex pairs. As $\Delta\Phi$ increases, cross-shear induced by oblique segments of the primary vortices in the braid region results in the formation of single secondary vortex strands. The flow is not receptive to spanwise phase variations with wavelengths shorter than the streamwise wavelength of the Kelvin–Helmholtz instability. When the phase variation is $\Delta\Phi = \pi$, the flow is excited with pairs of oblique waves only and undergoes a double rollup, resulting in the formation of spanwise-deformed vortices at twice the excitation frequency. Measurements of the streamwise velocity component show that the excitation leads to a substantial increase in the cross-stream spreading of the shear layer and that distortions of transverse velocity profiles are accompanied by an increase in the high-frequency content of velocity power spectra. Detailed schlieren visualizations shed light on the nature of 'vortex dislocations' previously observed by other investigators. Complex spanwise-non-uniform pairing interactions between the spanwise vortices are forced farther downstream by spanwise-amplitude or phase variations of subharmonic excitation wavetrains.

1. Introduction

Experimental investigations of nominally two-dimensional plane shear layers have suggested that substantial spanwise deformations of the primary vortices can result from relatively small disturbances in the free streams. Of particular note are the flow visualization photographs of Chandrsuda *et al.* (1978) that show spanwise-non-

uniform pairing and branching of the primary vortices, presumably due to non-uniform entrainment from the quiescent side of a single-stream mixing layer. Although global features of unforced single- and two-stream mixing layers may be somewhat different, similar spanwise irregularities of the primary vortices were also observed in two-stream mixing layers. Browand & Troutt (1980, 1985) detected vortex 'terminations' or 'branches' in time series of instantaneous spanwise profiles of the streamwise velocity. These patterns were attributed in a later paper (Browand & Ho 1987) to spanwise-non-uniform pairing interactions between adjacent primary vortices due to slight spanwise variations in the free-stream velocities. This and other experimental evidence (e.g. Keller *et al.* 1988; Delville *et al.* 1989) indicate that the characteristic spanwise wavelength of the deformations of the primary vortices is typically larger than the streamwise wavelength of the Kelvin–Helmholtz instability λ_{KH} of the base flow.

The evolution of the primary (spanwise) vortices in a plane mixing layer has been connected with the propagation and amplification of two-dimensional instability waves (e.g. Ho & Huerre 1984). The Strouhal number $St_n = \theta\nu_n/U_c$ of the most amplified wave corresponds to the natural frequency ν_n of the mixing layer, where θ is the momentum thickness, and the associated phase velocity U_c is equal to the average velocity of the two streams (linear stability theory suggests that $St_n = 0.032$). This implies that even small spanwise variations in U_c can lead to significant spanwise phase distortions of the unstable wavetrain and, as a result, to spanwise-non-uniform rollup and deformations of the ensuing primary vortices. Such deformations are apparent in the flow visualization photographs of Lasheras & Choi (1988), which were taken in a shear layer having spanwise-non-uniform free-stream velocity distributions.

Core deformations of the primary vortices can also be effected by the introduction of time-dependent spanwise phase perturbations at the trailing edge of the flow partition. Browand & Prost-Domasky (1990) and Dallard & Browand (1993) used a spanwise array of speakers to excite two adjacent spanwise segments of a two-stream mixing layer with time-harmonic wavetrains having slightly different frequencies. This excitation leads to the appearance of spanwise defects in time series of instantaneous spanwise profiles of the streamwise velocity that are similar to the unforced patterns previously observed by Browand & Troutt (1980, 1985). The defects first appear at spanwise positions corresponding to frequency discontinuities and are a precursor to the appearance of additional spanwise defects farther downstream. Because the two frequencies ν_2 and ν_1 are very close ($\nu_2 = 1.1\nu_1$), the two spanwise segments of the excitation waveform may be thought of as two almost identical wavetrains undergoing a slow time-periodic phase shift at the beat frequency $\nu_2 - \nu_1$. Hence, it may be argued that defects are formed at the beat frequency at spanwise phase discontinuities of the excitation waveform.

It is important to recognize that the measurements of Browand and his co-workers were taken at a fixed cross-stream elevation near the outer edge of the mixing layer (Browand & Troutt 1980, 1985; Browand & Prost-Domasky 1990) and thus are the footprints of three-dimensional vortical structures within the layer. Three-dimensional vortical structures in a plane wake were studied by Meiburg & Lasheras (1988, 1990) and the evolution of defects or dislocations in this flow was extensively investigated by Williamson (1989, 1992). Such structures were also observed by Nygaard & Glezer (1990, see also Nygaard 1991) in a two-stream mixing layer subjected to spanwise-periodic phase excitation. As a result of the excitation, the primary vortices undergo spanwise deformation having a spanwise wavelength which typically exceeds λ_{KH} and induce secondary vortical structures, the shape and strength

of which vary with the spanwise phase change $\Delta\Phi$. In particular, when $\Delta\Phi = \pi$, the primary vortices and the induced secondary vortices appear to be of comparable strength, and diamond-shaped vortex cells appear in the spanwise (x, z) plan view of the mixing layer.

Spanwise instability modes of the shear layer that can lead to core deformations of the primary vortices have also been studied analytically and numerically. In an analysis of a shear layer modelled by an array of Stuart vortices, Pierrehumbert & Widnall (1982) identified two such instability modes resulting from interaction of a pair of oblique time-harmonic wavetrains having equal amplitudes and opposite wave angles. The first mode, referred to as 'translative instability', is spanwise- and streamwise-periodic. The authors conjectured that the translative instability can lead to the formation of streamwise vortices which had been previously observed in the experiments of Breidenthal (1981). In a related study, Corcos & Lin (1984) showed that the rollup of spanwise vorticity into a streamwise-periodic array of vortices can give rise to a translative core instability which allows spanwise perturbations to grow in such a way that all spanwise vortices are identically distorted.

The second instability mode identified by Pierrehumbert & Widnall is subharmonic, can lead to spanwise-localized pairing of the primary vortices, and has a short-spanwise-wavelength cutoff, below which three-dimensional disturbances do not amplify. A similar instability was also observed in a numerical study of Ashurst & Meiburg (1988) and by E. Meiburg (personal communication, 1990) and is also apparent in the flow visualization of Lasheras & Choi (1988). In numerical simulations of a temporally evolving mixing layer, Comte & Lesieur (1991) investigated the evolution of the subharmonic instability and the topology of the streamwise vortices. They found that the introduction of small, random three-dimensional isotropic disturbances can lead to spanwise-non-uniform pairing of the primary vortices with a characteristic spanwise wavelength that is four times greater than the streamwise wavelength of the Kelvin–Helmholtz instability. The addition of two-dimensional disturbances leads to suppression of spanwise-non-uniform pairing, an in-phase waviness of the primary vortices, and the formation of streamwise vortices in the braid region.

That deformations of the primary vortices are an important ingredient in the evolution of the flow, even at high speeds, was demonstrated by direct numerical simulations of compressible mixing layers (Sandham & Reynolds 1991). Using random noise as the initial condition, the authors found that oblique waves (which lead to the formation of oblique primary vortices) are the most rapidly amplified instabilities for convective Mach numbers, $M_c > 0.6$. (While we are unaware of any other previous experiments in which a plane shear layer was forced with a time-harmonic oblique wavetrain, the low-speed experiments of Roos, Kegelman & Kibens 1989 in a shear layer facility having a flow partition with a swept trailing edge clearly demonstrate the receptivity of the flow to oblique disturbances.) Sandham & Reynolds further propose that the nonlinear development of a single oblique wave and pairs of equal and opposite oblique waves leads to the formation of oblique vortices and pairs of staggered lambda vortices, respectively.

The numerical and analytical investigations cited above clearly suggest that the plane shear layer is receptive to time-harmonic excitation having a spanwise-non-uniform phase distribution. Furthermore, experimental evidence indicates that spanwise phase distortion of two-dimensional instability modes can have dramatic effects on the rollup and evolution of the primary vortices. The present work builds on these findings and focuses on the evolution of three-dimensional vortical structures resulting from

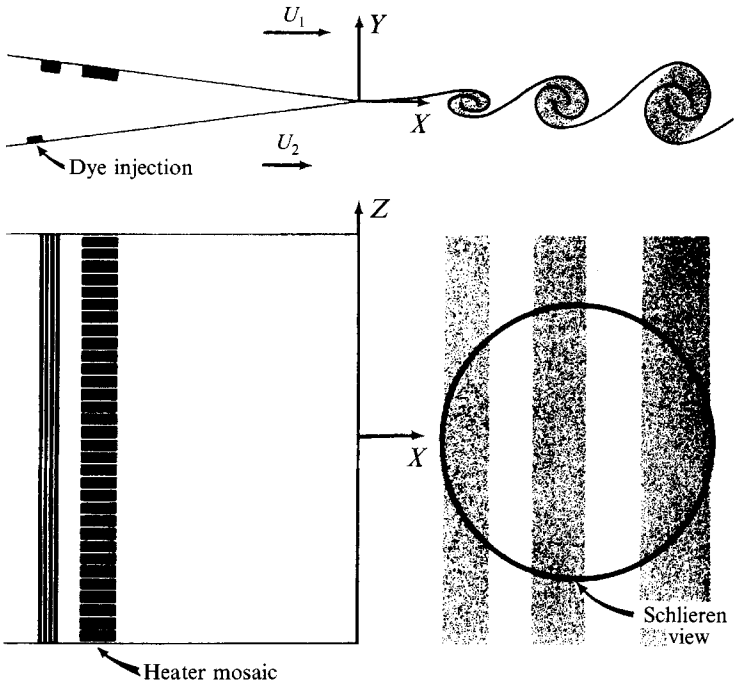

FIGURE 1. Schematic drawing of the flow partition, heater array, schlieren view, and coordinate system. The heater array is composed of four spanwise-continuous elements upstream of a linear array of 32 elements.

spanwise phase non-uniformities of the fundamental and subharmonic instabilities of the base flow. Section 2 contains a description of the experimental apparatus, the surface actuators used for synthesis of the excitation waveforms, and several programmes of spanwise-non-uniform phase excitation. The response of the mixing layer to fundamental and subharmonic phase excitation is described in §3, with emphasis on spanwise-linear and spanwise-periodic phase distributions. Concluding remarks are presented in §4.

2. Experimental apparatus and techniques

2.1. *The experimental set-up*

The closed-return water shear layer facility and the ancillary diagnostic equipment are described in detail by Nygaard & Glezer (1991) (hereafter referred to as N&G). Excitation of streamwise and spanwise instability modes is accomplished by a linear spanwise array of 32 heating elements flush-mounted on the high-speed side of the flow partition (similar arrays of surface film heaters were used by Robey 1987 and Schneider 1989 for the excitation of oblique waves in a flat-plate boundary layer). Each of the heating elements is wired to a DC power amplifier and can be independently driven from the laboratory computer via a D/A interface. The flow partition, heater mosaic, and coordinate system are shown schematically in figure 1. The heater mosaic is composed of four spanwise-uniform elements and a single 32-element spanwise array. The spanwise width of the mosaic is 22 cm and is equal to the spanwise of the test section. The refractive index gradients produced by surface heating are exploited for flow visualization by means of a sensitive schlieren system. The schlieren view is in the

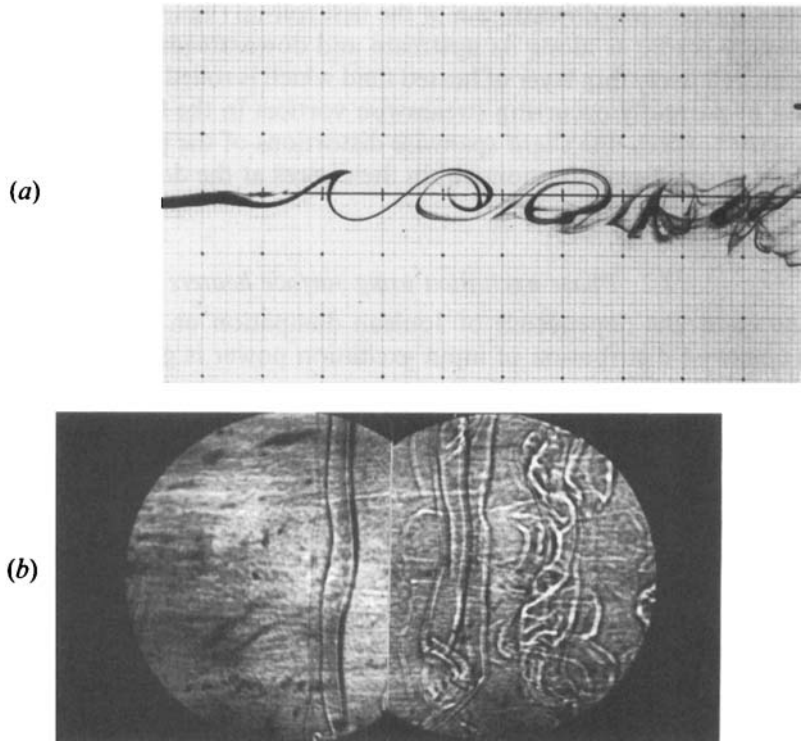

FIGURE 2. Side (x, y) and plan (x, z) views of the shear layer subjected to spanwise-uniform time-harmonic excitation. The side (*a*) and plan (*b*) views are dye (injected at midspan) and schlieren visualizations, respectively. The two photographs have the same scale and were taken at the same phase relative to the excitation waveform. The flow is from left to right, and the free-stream velocities are 30 and 10 cm s^{-1}. The grid in (*a*) is square and measures 2.54 cm on the side. The plan view in (*b*) is 20.2 cm long and 13.2 cm wide (in the x- and z-directions, respectively). Its upstream edge begins at $x = 1$ cm.

spanwise (x, y)-plane, consists of a circle 13.2 cm in diameter centred at midspan, and may be thought of as a planar projection of streaklines of slightly heated fluid elements. The flow is also visualized by dye. Fifteen equally spaced injection ports are available on each side of the flow partition. Simultaneous cross-stream or spanwise measurements of the streamwise velocity component are taken with a rake of 31 hot-wire probes, 2 mm apart, suitable for use in water.

The response of the flow to spanwise-uniform time-harmonic excitation was extensively documented by N&G. In figure 2(*a*, *b*) the excitation frequency is 5 Hz and the flow is photographed in the cross-stream (x, y)- and spanwise (x, z)-planes. Figure 2(*a*, *b*) is identical to figure 6(*a*, *b*) of N&G and is reproduced here for reference. The two photographs have the same scale and are taken at the same phase relative to the excitation waveform. The flow is from left to right, and the free-stream velocities are $U_1 = 30$ cm s^{-1} and $U_2 = 10$ cm s^{-1}. In the (x, y)-plane (figure 2*a*), the flow is visualized by dye that is injected at midspan into the boundary layer of the low-speed stream.

Figure 2(*b*) is a composite of two partially overlapping phase-locked schlieren views in the (x, z)-plane, which are centred at 7.6 cm and 15.2 cm downstream of the trailing edge of the flow partition so that in the composite view $1 \leqslant x \leqslant 21.8$ cm (or $0.25 \leqslant X \leqslant 5.45$, where $X = Rx/\lambda_{KH}$, $R = (U_1 - U_2)/U_c$). At this excitation frequency, pairing of the primary vortices is inhibited in the streamwise domain shown here. The

primary vortex immediately downstream of the first roll-up (figure 2*b*) is characterized by sharp intensity gradients along its upstream and downstream edges caused by the curvature of the relatively thin layer of heated fluid which is rolled into the vortex. Note the formation of naturally occurring streamwise vortices in the braid region between adjacent primary vortices, the slight spanwise distortions of the primary vortices, and the appearance of small-scale motion within their cores at the downstream end of the composite schlieren view.

2.2. *Phase excitation using surface heaters*

Owing to the quadratic dependence of Joulean dissipation on input voltage to the heaters, the spanwise distribution of input excitation power is given by

$$E(z,t) = E_0(z)\{1+\cos[2\pi\nu(z)\,t+\Phi(z)]\},$$

where $E_0(z)$ is the mean power, $\nu(z)$ is the spanwise distribution of excitation frequency, and $\Phi(z)$ is the spanwise phase distribution. The linear heater array described in §2.1 is used to synthesize a 32-element discretization of $E(z,t)$, where $E_0(z)$, $\nu(z)$, and $\Phi(z)$ are, in principle, arbitrary and can be programmed from the laboratory computer. While in the experiments of N&G, $E_0(z)$ was spanwise-periodic and $\nu(z)$ and $\Phi(z)$ were spanwise-uniform, the present experiments employ three phase programmes by varying the phase and frequency of a time-harmonic excitation wavetrain having a constant amplitude:

(i) spanwise-linear phase distribution denoted Φ_{LIN} (§2.2.1),

(ii) spanwise-periodic phase distribution denoted Φ_{SP} (§2.2.2),

and

(iii) time- and spanwise-periodic phase distribution denoted Φ_{TSP} (§2.2.3) (spanwise-uniform phase distribution is referred to as Φ_{SU}).

Near the flow partition, phase distortions of the excitation wavetrain result in spanwise-non-uniform rollup and deformations of the primary vortices and in the concomitant evolution of secondary vortical structures (§§3.1–3.4). The present work also shows that phase deformations can continue to occur downstream of the initial rollup of the fundamental (Kelvin–Helmholtz) instability as a result of spanwise-non-uniform pairing interactions of the primary vortices. These pairing interactions are induced by a superposition of fundamental and subharmonic excitation wavetrains where the fundamental wavetrain is spanwise-uniform and the subharmonic has spanwise-periodic phase and amplitude programs Φ_{SP-sh} and E_{SP-sh}, respectively (§3.6).

Finally, the effect of phase distortions on secondary counter-rotating vortex pairs that are triggered by upstream (amplitude) disturbances on the flow partition are studied using a linear superposition of two fundamental wavetrains having either spanwise-periodic amplitude (E_{SP}) or phase (Φ_{SP}) distributions (§3.5).

2.2.1. *Spanwise-linear phase excitation* Φ_{LIN}

Spanwise-linear phase distribution $\Phi(z) = \beta z$ (where $\beta = \text{const}$) results in the excitation of a time-harmonic oblique wavetrain having a spanwise wavenumber β. When Φ_{LIN} is synthesized using a 32-element discretization by the linear heater array, $E(z)$ is effectively piecewise-constant with phase increments $\Delta\Phi$ between adjacent heater elements (Robey 1987; Schneider 1989). In the present experiments $\beta \leqslant 0.93\ \text{cm}^{-1}$ and thus $\Delta\Phi \leqslant 6\pi/32$. The response of the shear layer to excitation with oblique waves is discussed in §3.1.

2.2.2. *Spanwise-periodic phase distribution* Φ_{SP}

When $\Phi(z)$ is spanwise-periodic and piecewise constant, $E(z,t)$ is a linear superposition of a time-harmonic spanwise-uniform wavetrain and pairs of equal and opposite oblique waves. A spanwise-periodic and piecewise-constant phase distribution can be easily discretized by the heater array for any spanwise wavelength λ_z that is equal to the width of an integer number of heating elements. To define $\Phi(z)$, let $z = z_0 + \lambda_z s$, where z_0 is an arbitrary reference, λ_z is the spanwise wavelength, and $0 \leqslant s \leqslant 1$. Then, in each wavelength, $\Phi(z) = 0$ for $0 \leqslant s \leqslant s_1$ and $s_2 \leqslant s \leqslant 1$ (where $s_1 < s_2$) and $\Phi(z) = \Delta\Phi$ for $s_1 \leqslant s \leqslant s_2$. In the present experiments, λ_z is taken to be the width of 2, 4, 8, and 16 elements of the linear heating array, $s_2 - s_1 = 0.5$, and $0 \leqslant \Delta\Phi \leqslant \pi$.

With a spanwise-periodic phase distribution, $E(z,t)$ can be expanded in Fourier series,

$$E(z,t) = E_0[1 + e(z,t)],$$

where

$$e(z,t) = \cos(\tfrac{1}{2}\Delta\Phi)\cos(\omega t + \tfrac{1}{2}\Delta\Phi) + \sin(\tfrac{1}{2}\Delta\Phi)\sin(\omega t + \tfrac{1}{2}\Delta\Phi)\sum_{n=1}^{\infty}\frac{4}{\pi(2n-1)}\sin\left(\frac{2(2n-1)\pi}{\lambda_z}z\right).$$

Thus, for a given $\Delta\Phi$, $E(z,t)$ is a linear superposition of a time-harmonic spanwise-uniform wavetrain and pairs of equal and opposite oblique waves having spanwise wavenumbers $\beta_n = 2(2n-1)\pi/\lambda_z$. The amplitudes of the spanwise-uniform and oblique wavetrains are proportional to $\cos(\frac{1}{2}\Delta\Phi)$ and $\sin(\frac{1}{2}\Delta\Phi)$, respectively (note that the amplitudes of each pair of oblique waves also decrease like $1/n$). Hence, when $\Delta\Phi = 0$, $E(z,t)$ *is a spanwise-uniform wavetrain* and when $\Delta\Phi = \pi$, $E(z,t)$ *is a superposition of pairs of equal and opposite oblique waves only*. A similar Fourier decomposition of a time-harmonic excitation wavetrain having a spanwise-periodic phase distribution was also used in the numerical simulations of Collis *et al.* (1991).

As shown in §3.2, when $\Delta\Phi = \pi$, there exists a short-wavelength cutoff, λ_{crit}, below which $E(z,t)$ is not amplified. Thus, it may be argued that there is a corresponding cutoff spanwise wavenumber, β_{crit}, such that pairs of equal and opposite oblique waves are attenuated when $\beta_n \geqslant \beta_{crit}$. Hence, when λ_z is small, $E(z,t)$ is effectively a linear superposition of a two-dimensional wavetrain and a single pair of oblique waves, all at the same (excitation) frequency.

2.2.3. *Spanwise- and time-periodic phase distribution* Φ_{TSP}

Piecewise-constant and spanwise-periodic (with wavelength λ_z) frequency distributions of the excitation wavetrain are used to approximate spanwise-periodic phase distributions where the phase difference between adjacent segments of the excitation waveform is slowly varying with time. Time-harmonic excitation wavetrains with piecewise-constant frequency distributions were used by other investigators (e.g. Browand and coworkers; Williams-Stuber & Gharib 1989) to effect dislocations of the primary vortices in a plane shear layer. If the spanwise frequency variation is $\Delta\nu = \nu_2 - \nu_1$ where ν_1 and ν_2 are the two (piecewise-constant) frequencies of adjacent segments of the excitation waveform, then the phase difference between these segments may be thought of as $\Delta\Phi = 2\pi(\nu_2 - \nu_1)t$ if $\Delta\nu/\nu_2 \ll 1$. This phase difference is varying with time between 0 and 2π over the beat period $1/\Delta\nu$ on a timescale that is much longer than the period of either forcing frequency.

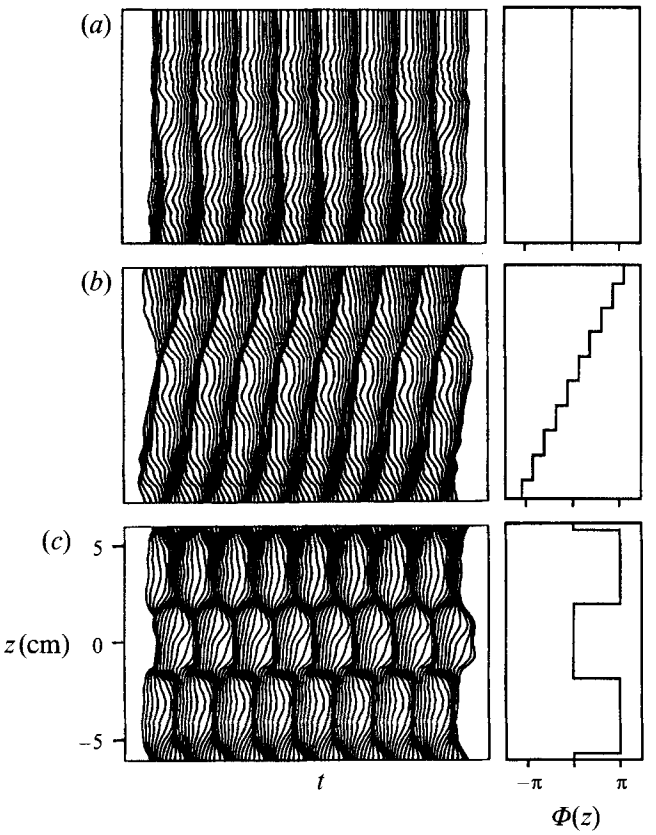

FIGURE 3. Time plots of spanwise distributions of $\langle u_{pert}(z,t)\rangle$ measured at $x = 5.1$ cm at the cross-stream elevation where $U(x) = 20$ cm s^{-1}. The origins of successive profiles of $\langle u_{pert}(z,t)\rangle$ are equally displaced in time: (*a*) Φ_{SU}; (*b*) Φ_{LIN} with $\beta = 0.62$ rad cm^{-1}; (*c*) Φ_{SP} with $\lambda_z = 7.62$ cm, and $\Delta\Phi = \pi$. The respective spanwise phase distribution is shown to the right of each plot.

It is noted, however, that there is a fundamental difference between the evolution of the primary vortices depending on whether the time-harmonic excitation has piecewise-constant frequency or phase distributions. The circulation per unit streamwise length in the cross-stream plane of a nominally two-dimensional shear layer is spanwise-uniform, and the circulation over the streamwise wavelength of the two-dimensional instability λ_{KH}, is $\Gamma \approx \Delta U \lambda_{KH}$. Hence, in a shear layer that is forced with a time-harmonic wavetrain having a piecewise-constant frequency distribution, the excitation wavelengths on either side of the frequency discontinuity are not equal and, consequently, while the circulations of adjacent segments of the primary vortices are time-invariant, they are not the same (e.g. Nassef & Browand 1993). On the other hand, when $\nu = \text{const}$ and $\Phi(z)$ is piece-wise-constant (§2.2.2), Γ is spanwise-uniform.

Because $\Gamma_2/\Gamma_1 = 1 - \Delta\nu/\nu_2$, the spanwise variation in the cross-stream circulation of the primary vortices diminishes with $\Delta\nu$. In most of the present work, $\nu_1 = 4.9$ Hz and $\nu_2 = 5.0$ Hz, so that the beat period is 10 s, $\Delta\nu/\nu_2 = 0.02$, and $\Gamma_2/\Gamma_1 = 0.98$. Hence, in spite of the slight spanwise variations in cross-stream circulation, it may be argued that the structure of the shear layer for a given spanwise-periodic and piecewise-constant phase distribution is virtually the same regardless of whether the excitation phase programme is Φ_{SP} or Φ_{TSP}.

	Programme	U_2/U_1 (cm s^{-1})		
1	Φ_{LIN}	30/10	$\alpha = 1.57$ cm^{-1}, $\beta = 0.31, 0.62, 0.93$ cm^{-1}	§3.1
2	Φ_{TSP}	30/10	$\nu_1 = 4.9$ Hz, $\nu_2 = 5$ Hz, $\lambda_z = 7.6$ cm, $\lambda_z/\lambda_{KH} \approx 1.9$	
3	Φ_{TSP}	36/12	$\nu_1 = 6.9$ Hz, $\nu_2 = 7$ Hz, $\lambda_z = 7.6$ cm, $\lambda_z/\lambda_{KH} \approx 2.2$	§3.2
4	Φ_{SP}	30/10	$\nu = 5$ Hz, $6.25 \geqslant \lambda_z \geqslant 1.27$, $1.6 > \lambda_z/\lambda_{KH} > 0.3$	
5	Φ_{TSP}	30/10	$\nu_1 = 4.9$ Hz, $\nu_2 = 5$ Hz, $\lambda_z = 10.2$ cm, $\lambda_z/\lambda_{KH} \approx 2.5$	§3.3
6	Φ_{SP}	30/10	$\nu = 5$ Hz, $\lambda_z = 5.1$ cm, $\lambda_z/\lambda_{KH} \approx 1.3$	
7	Φ_{TSP}	30/10	$\nu_1 = 4.9$ Hz, $\nu_2 = 5$ Hz, $\lambda_{KH} \approx 4$ cm	§3.4
8	E_{SP}	30/10	$\nu = 5$ Hz, $\lambda_z = 5.1$ cm, $\lambda_z/\lambda_{KH} \approx 1.3$	§3.5
9	Φ_{SP}	30/10		
10	E_{SP-sh}	42/14	$\nu = 9$ Hz, $\lambda_z = 20.3$ cm, $\lambda_z/\lambda_{KH} = 6.5$	§3.6
11	Φ_{SP-sh}	42/14		

TABLE 1. Phase programmes and corresponding experimental conditions

2.3. *Effect of phase excitation on the flow*

The response of the flow to phase excitation near the trailing edge of the flow partition is shown in time plots of ensemble-averaged spanwise distributions of the streamwise velocity perturbation, $\langle u_{pert}(z,t)\rangle$ (figure 3*a–c*). (The ensemble-averaged streamwise velocity $\langle u(x,t)\rangle$ is phase-locked to $E(z,t)$ and $\langle u_{pert}(x,t)\rangle = \langle u(x,t)\rangle - U(x)$, where $U(x)$ is the mean flow velocity.) These data are measured at $x = 5.1$ cm and $y = y_0$ (y_0 is the cross-stream elevation where $U(x) = U_c = \frac{1}{2}(U_1 + U_2)$). In figure 3, the origins of successive profiles are equally displaced in time, producing (z,t)-maps that capture spanwise features of the forced flow before the rollup of the primary vortices is completed. The centres of the dark bands correspond to extrema of $\langle u_{pert}(z,t)\rangle$. The corresponding spanwise phase distribution of the excitation waveform is shown to the right of each time plot.

When the phase of the excitation waveform is spanwise uniform (Φ_{SU}, figure 3*a*), the flow appears to be reasonably two-dimensional. The dark bands in the (z,t)-maps have been associated by Browand and his co-workers with the passage of the primary vortices (Browand & Troutt 1980, 1985; Browand & Prost-Domasky 1990). In figure 3(*b*), the excitation programme is Φ_{LIN}, $\Phi(z) = \beta z$, where $\beta = 0.62$ cm^{-1} and results in a spanwise-oblique phase distribution of $\langle u_{pert}(z,t)\rangle$. Furthermore, the dark bands in the (z,t)-map imply the rollup of oblique primary vortices. In figure 3(*c*), the phase distribution is spanwise-periodic Φ_{SP} with $\Delta\Phi = \pi$, $\lambda_z = 7.62$ cm (i.e. equal to the width of 12 heating elements) such that $\Phi = 0$ at the centre 6 elements. This excitation waveform corresponds to a family of equal and opposite oblique waves (§2.2.2), and leads to spanwise-periodic phase discontinuities of $\langle u_{pert}(z,t)\rangle$ at the excitation wavelength, λ_z. Figure 3(*c*) suggests that rollup of the primary vortices occurs in spanwise segments of constant phase.

The phase programs and corresponding experimental conditions that are used throughout the present manuscript are summarized in table 1.

3. Spanwise-non-uniform phase excitation

As discussed in §1, experimental observations indicate that phase distortions of the nominally two-dimensional instability modes in a plane shear layer can lead to

significant distortions of the ensuing primary and secondary vortical structures. In most of these investigations, phase distortions resulted from unknown (and uncontrolled) disturbances in the free streams. Controlled excitation of phase disturbances in the plane shear layer has been limited to time-periodic phase distortions by means of spanwise variations of the forcing frequency (Browand & Prost-Domasky 1990; Nassef & Browand 1993) and to passive excitation of oblique instability modes by means of geometrical alterations in the flow partition (Roos *et al.* 1989).

The present investigation focuses on the effect of controlled phase excitation on the evolution of the primary and secondary vortices. Near the flow partition, phase distortions of the excitation wavetrain result in spanwise-non-uniform rollup and thus in deformations of the primary vortices that persist throughout the present domain of observation; these are discussed in §§3.1–3.5. Experimental evidence (Browand & Ho 1987; Keller *et al.* 1988; Delville *et al.* 1989) indicates that phase distortion of the base flow is not merely a near-field phenomenon and, given its characteristic spanwise wavelength, it appears to be connected with amplification of subharmonic modes. Thus, it is conjectured that far downstream of the flow partition, the excitation is effected through the amplification of a hierarchy of fundamental and subharmonic instability modes of the two-dimensional base flow. In §3.6 it is shown that phase distortions and deformations of the nominally two-dimensional base flow can continue to recur far downstream from the flow partition through spanwise-non-uniform subharmonic (pairing) interactions of the primary vortices.

In most of the present experiments, the free-stream velocities are 30 and 10 cm s^{-1} and the excitation frequency is 5 Hz. The streamwise domain of observation is $1 \leqslant x \leqslant 21.8$ cm, or $0.25 \leqslant X \leqslant 5.45$ where $X = Rx/\lambda_{KH}$, $R = (U_1 - U_2)/U_c$. The measurements of N&G were taken up to $x = 25.4$ cm (i.e. $X = 6.35$) where $x/\theta_{te} \approx 423$ (θ_{te} is the momentum thickness at the trailing edge of the flow partition) and where the Reynolds number based on the local momentum thickness of the unforced flow is $Re_\theta = 1450$. It is also noted that typical Reynolds numbers associated with small-scale transition in liquid shear layers fall in the range $750 < Re_\theta < 1700$ (Ho & Huerre 1984).

3.1. *Spanwise-linear phase excitation*

The effect of a spanwise-linear phase distribution, $\Phi(z) = \beta(z - z_0)$ (where z_0 is an arbitrary reference), is studied using flow visualization. The resulting excitation waveform is a time-harmonic oblique wavetrain (shown schematically in figure 4*a*) having streamwise and spanwise wavenumbers, $\alpha = 2\pi\nu/U_c$ and β. In the present experiments, $\alpha \approx 1.57$ cm^{-1} and the responses of the flow to excitation with $\beta = 0.31$, 0.62, and 0.93 cm^{-1} are shown in figure 4(*b*, *c*, *d*), respectively. The corresponding wave angles, $\psi = \arctan(\beta/\alpha)$, between the wave vectors and the streamwise direction are 11.2°, 21.5°, and 30.6° (in what follows, $\psi > 0$ if $\beta > 0$). It should be recognized that, unlike excitation of two-dimensional waves, the excitation of oblique waves in a two-dimensional base flow gives rise to a three-dimensional vorticity perturbation field with important consequences for the evolution of the excited flow. This was demonstrated for a flat-plate boundary layer by Hama *et al.* (1987), and by Robey (1987).

The most striking feature in figure 4(*b–d*) is the formation of primary vortices that are oblique in the spanwise (x, z)-plane of the shear layer and are advected in the streamwise direction. The angles between the oblique vortices and the streamwise direction are virtually identical to the corresponding wave angles of the excitation wavetrains and remain almost invariant throughout the streamwise domain shown here. In what follows, successive primary vortices downstream from the flow partition

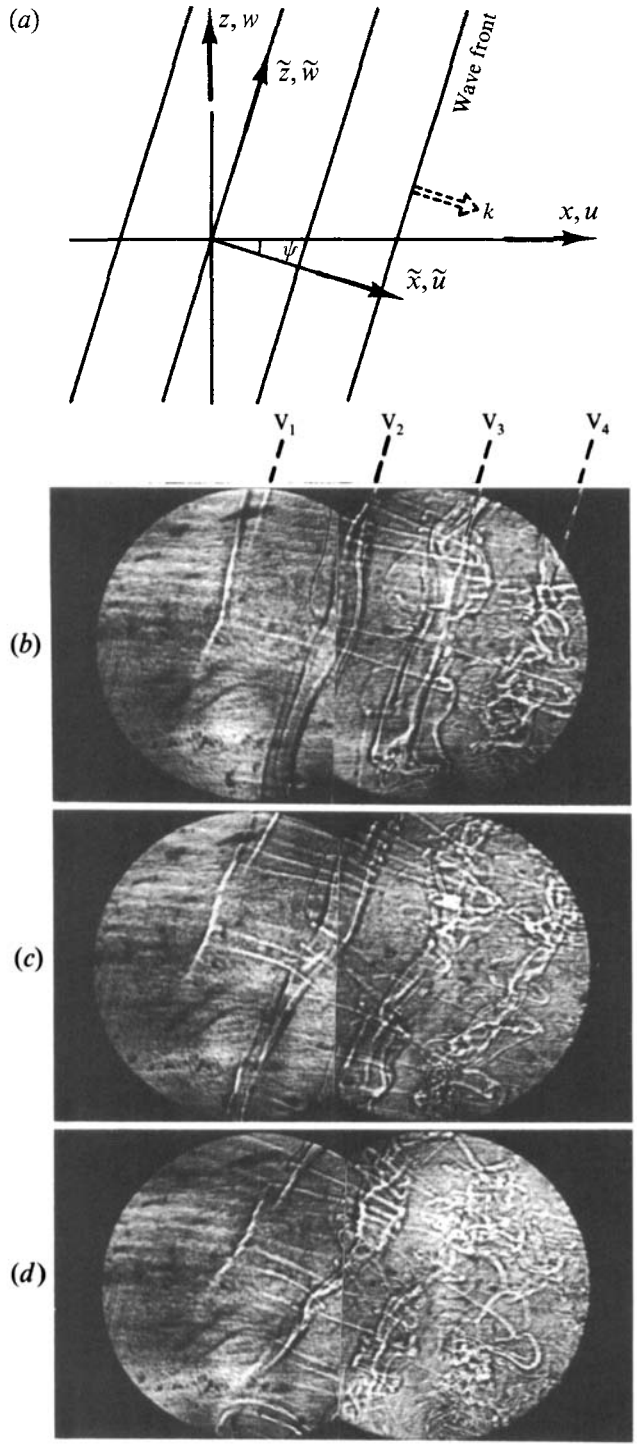

FIGURE 4. Excitation with spanwise-linear phase distribution. Schematic drawing of the oblique wavetrain is shown in (*a*); the response of the flow to excitation with $\alpha = 2\pi\nu/U_c \approx 1.57\ \mathrm{cm}^{-1}$ and $\beta = 0.31$, 0.62, and $0.93\ \mathrm{cm}^{-1}$ ($\psi = 11.2°$, 21.5°, and 30.6°, respectively) is shown in the (x, z) composite schlieren photographs (*b*), (*c*), and (*d*), respectively.

are referred to below and in figure 4(*b–d*) as V_1, V_2, V_3 etc. As can be seen on the left-hand side of each photograph, the rollup of V_1 occurs along a line of constant phase of the excitation wavetrain. The rollup clearly does not occur simultaneously along the axis of each vortex, as for the two-dimensional case, but progresses obliquely as the vortex is advected downstream.

It is apparent from the present and other flow visualization photographs that the rollup at any position along the axis of V_1 in figure 4(*b–d*) starts at the same streamwise station, $x = x_r$. Furthermore, because x_r is approximately the same in each of figures 4(*b*)–4(*d*), it may be concluded that spatial amplifications of all oblique waves over the range of spanwise wavenumbers considered here are almost identical. When β exceeds 0.93 cm^{-1}, it is observed that the flow is no longer locked to the excitation wavetrain and a streamwise-regular pattern of oblique vortices does not exist. This, however, does not necessarily imply that, for $\beta > 0.93$ cm^{-1}, oblique waves are not amplified in the plane shear layer because, in the present experiments, the receptivity of the flow-partition boundary layers is inherently coupled to that of the ensuing shear layer. The results of Schneider (1989) indicate that the amplitude of oblique waves in a flat-plate (Blasius) boundary layer measured at a streamwise position corresponding to $Re_{\delta^*} = 1300$ is almost invariant for $\psi < 15°$, and decreases by an order of magnitude for $15° < \psi < 25°$.

The streamwise inclination of the primary vortices is apparently accompanied by a change in the direction of the strain field in the braid region between them, compared to the two-dimensional case. As a result, secondary vortices that are formed in the braid region are approximately aligned with the wave vector of the excitation wavetrain. In the absence of phase excitation, only a few weak secondary vortices appear in the braid region between V_1 and V_2 (see figure 2*b*). However, as β is increased, secondary vortex pairs in the braid region between V_1 and V_2 become more pronounced (e.g. figure 4*b*, *c*). These vortex pairs are clearly associated with the rollup of V_1 in that they continue to form in the braid region as the rollup of V_1 progresses. While the amplitude of $E(z, t)$ is spanwise-uniform, Φ_{LIN} is piecewise-constant due to a 16-element discretization, which leads to spanwise phase discontinuities, $\Delta\Phi = 1.27\beta$, each having a spanwise width equal to the width of two heating elements (12.7 mm). Although the secondary vortices are formed only after the rollup of V_1, they are clearly triggered by spanwise discontinuities of the excitation waveform, as is evident from their spanwise spacings and apparent strength.

The formation and orientation of the secondary vortices are extremely sensitive to deformations along the axes of the primary vortices, as can be seen in the braid regions between V_2 and V_3 in figure 4(*c*, *d*). The primary vortices appear to be more susceptible to such deformations as β is increased, and the characteristic wavelength of these deformations is longer than the streamwise wavelength of the Kelvin–Helmholtz instability. When $\beta = 0.93$ cm^{-1} (figure 4*d*), the primary vortex at the downstream edge of the schlieren view exhibits a bifurcation that is also apparent in the photograph of Chandrsuda *et al.* (1978, their figure 3). Similar bifurcations can also be inferred from the data of Browand & Prost-Domasky (1990) and were observed by Nygaard & Glezer (1990) as a result of spanwise-non-uniform phase excitation. As will be shown in the following subsections, such deformations can arise from interactions between two-dimensional and oblique instability waves.

We next consider the temporal evolution of a train of oblique vortices resulting from excitation by an oblique wavetrain in an unbounded two-stream two-dimensional shear layer. If $\tilde{x}$ is taken to be parallel to the wave vector of the excitation wavetrain, $\tilde{y}$ is the cross-stream coordinate, and $\tilde{z}$ is normal to the $(\tilde{x}, \tilde{y})$-plane (i.e. parallel to the

axes of the oblique vortices, see figure 4*a*). Then the velocity and vorticity components in the $\tilde{z}$-direction, $\tilde{w}$ and $\tilde{\zeta}$, are given by

$$\frac{\mathrm{D}}{\mathrm{D}t}\tilde{w} = \left[\frac{\partial}{\partial t} + \tilde{\boldsymbol{u}}\cdot\tilde{\boldsymbol{\nabla}}\right]\tilde{w} = \nu\left[\frac{\partial^2\tilde{w}}{\partial\tilde{x}^2} + \frac{\partial^2\tilde{w}}{\partial\tilde{y}^2}\right]$$

and

$$\frac{\mathrm{D}}{\mathrm{D}t}\tilde{\zeta} = \left[\frac{\partial}{\partial t} + \tilde{\boldsymbol{u}}\cdot\tilde{\boldsymbol{\nabla}}\right]\tilde{\zeta} = \nu\left[\frac{\partial^2\tilde{\zeta}}{\partial\tilde{x}^2} + \frac{\partial^2\tilde{\zeta}}{\partial\tilde{y}^2}\right]$$

respectively (S. C. Crow, personal communication, 1992). These equations imply that, in the absence of viscosity, the $\tilde{z}$-velocity and vorticity components of fluid elements within the primary vortices and in the braid region remain unchanged. Because the oblique vortices are advected in a shearing flow, their induced velocity field acts to move high-speed (or low-speed) fluid down (or up) from higher (or lower) cross-stream elevations toward the braid region. The streamwise velocity of the fluid that is moved from the free streams has components in the $\tilde{z}$- and $\tilde{x}$-directions thus establishing a secondary shear layer across the braid region in the $\tilde{z}$-direction due to the cross-stream difference in $\tilde{w}$. Therefore, it appears that if the secondary oblique shear layer is strong enough, it may lead to the respective strengthening and weakening of the counter-rotating legs of the secondary lambda vortices and to the formation of single clockwise or counterclockwise secondary vortex strands. The formation of clockwise or counterclockwise secondary vortex strands as a result of cross-shear has also been reported by Atsavapranee & Gharib (1994) in a time-developing stratified mixing layer and is further discussed in §§3.2 and 3.4.

3.2. *Spanwise-periodic phase excitation: effects of* $\Delta\Phi$ *and* λ_z

When the phase distribution of the excitation waveform is spanwise-periodic and piecewise-constant, $E(z,t)$ is a linear superposition of a time-harmonic spanwise-uniform wavetrain and pairs of equal and opposite oblique waves having spanwise wavenumbers $\beta_n = (2n-1)\,2\pi/\lambda_z$ (cf. §2.2.2). In particular, recall that, when $\Delta\Phi = 0$ or π, $E(z,t)$ is a spanwise-uniform wavetrain or a superposition of pairs of oblique waves, respectively. In this section, we discuss the effects of $\Delta\Phi$ and λ_z on the evolution of the flow.

Figure 5(*a–i*) is a sequence of (x,z) composite Schlieren photographs (as in figure 2*b*) for which the phase programme of the excitation wavetrain is Φ_{TSP} (cf. §2.2.3) where the spanwise wavelength is $\lambda_z = 7.6$ cm, and the (piecewise-constant) frequencies of the excitation wavetrain are $\nu_1 = 4.9$ Hz and $\nu_2 = 5.0$ Hz. The photographs are taken phase-locked to the beat frequency $\nu_2 - \nu_1$ at 1 s intervals around the time corresponding to $\Delta\Phi = \pi$ (half the beat period, figure 5*e*). The corresponding increments in $\Delta\Phi$ are 0.2π. The piecewise-constant frequency distribution of the excitation wavetrain is ν_1 for $2(j-1)\,\lambda_z/2 < z < (2j-1)\,\lambda_z/2$ and ν_2 for $(2j-1)\,\lambda_z/2 < z < j\lambda_z$, where $j = 1, 2, \ldots$ and $\nu(z)$ is symmetric about midspan. In the (x,z) plan view of figure 5(*a–i*), the frequency of the centre segment of the excitation wavetrain ($-1.9 < z < 1.9$ cm) is 4.9 Hz. Phase-locking is accomplished by a conditional trigger derived from a logical 'AND' of two pulse trains each corresponding to zero-crossings (with a positive time derivative) of one of the excitation wavetrains. The resulting pulse train has a frequency $\nu_2 - \nu_1$ and is time-delayed to achieve a desired phase relative to the data acquisition clock.

At a given time, say $t = t_0$, the wave fronts of all segments of the excitation waveform are in phase. Because the frequency of the centre segment is slightly lower ($\nu_1 = 4.9$ Hz) than the frequency of the two adjacent (outer) segments, the centre segment of the

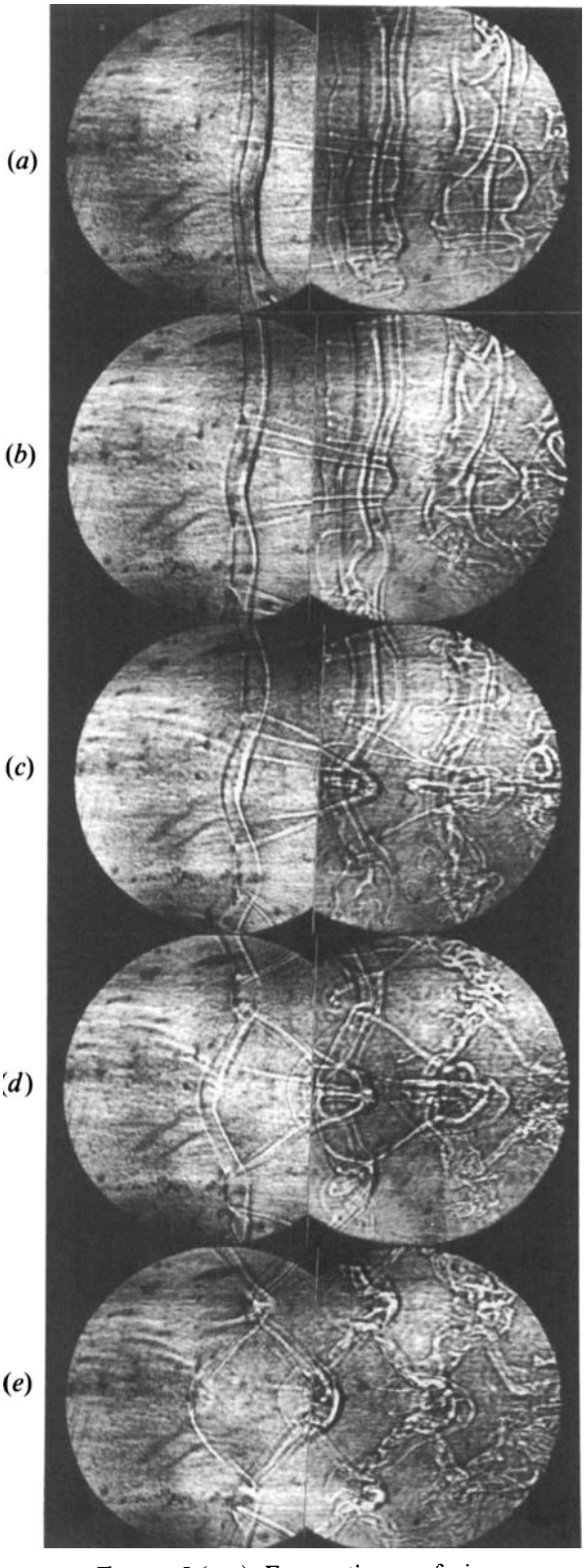

FIGURE 5 (*a–e*). For caption see facing page.

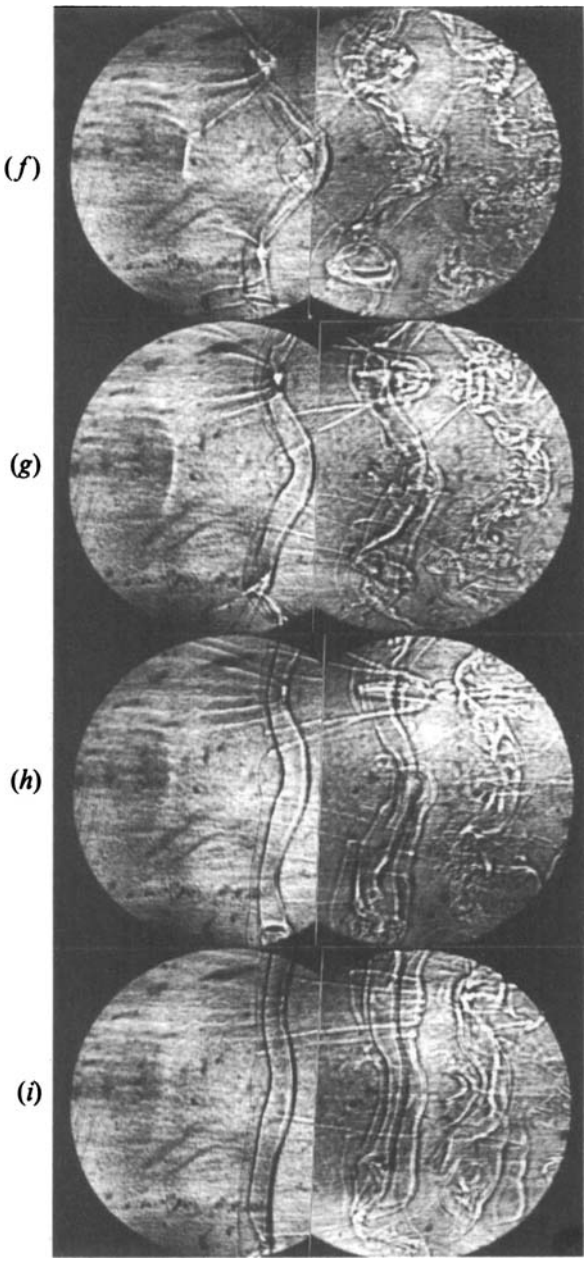

FIGURE 5. Excitation with time- and spanwise-periodic phase distribution Φ_{TSP} ($\nu_1 = 4.9$ Hz, $\nu_2 = 5.0$ Hz, and $\lambda_z = 7.6$ cm). The (x, z) composite schlieren photographs were taken phase-locked to the beat frequency of the two excitation wavetrains at 1 s time intervals. The frequency of the centre segment ($-1.9 < z < 1.9$ cm) is 4.9 Hz, and $\Delta\Phi$ is: (*a*) 0.2π, (*b*) 0.4π, (*c*) 0.6π, (*d*) 0.8π, (*e*) π, (*f*) 1.2π, (*g*) 1.4π, (*h*) 1.6π, and (*i*) 1.8π.

excitation waveform develops a phase lag with respect to the outer segments when $t > t_0$. Because the difference between ν_2 and ν_1 is small, streamwise amplifications of adjacent segments of the excitation wavetrain are virtually identical, and the subsequent rollup of corresponding segments of the primary vortices occurs at different times at

the same streamwise position downstream of the flow partition. As a result of the spanwise-non-uniform rollup, adjacent spanwise segments of the primary vortices become distorted at spanwise positions corresponding to phase discontinuities of $\Phi(z)$. When $\Delta\Phi < \pi$ (figure 5*a–d*), the centre segment of the excitation waveform lags in phase relative to the outer segments, and the primary vortices develop an upstream bend around midspan. When $\Delta\Phi > \pi$ (figure 5*f–i*), the centre segment leads in phase relative to the outer segments, and the primary vortices develop a downstream bend about midspan. For example, in figure 5(*g*), the centre segment of the excitation waveform leads in phase relative to the outer segments, and the rollup of the centre segment of the primary vortex (on the left-hand side) occurs before the rollup of the outer segments.

The deformations of the primary vortices are clearly proportional to the magnitude of $\Delta\Phi$. Even when $\Delta\Phi$ is relatively small (figures 5*a*, *b*, 5*h*, *i*), the undulations of the primary vortices persist and even appear to intensify with downstream distance. Because the primary vortices in an unforced plane mixing layer are advected in a nominally two-dimensional strain field, they deform in a plane that is aligned with the direction of maximum strain, and the amplitudes of their deformations can increase with downstream distance. An important consequence of these deformations is the appearance of secondary vortex strands that connect upstream and downstream bends of consecutive primary vortices through the braid region. These vortices are formed as a result of the spanwise discontinuities in the excitation waveform, and their evolution is affected by flow along the oblique segments of the primary vortices as discussed in more detail in §3.4. When $\Delta\Phi$ is relatively small (e.g. figures 5*b*, 5*h*), a pair of secondary vortices appears on each side of an upstream (or downstream) bend of the primary vortices. (The formation of multiple secondary vortices near spanwise distortions of the primary vortices was also observed by Lasheras, Cho & Maxworthy 1986 and by N&G.) As $\Delta\Phi$ increases (figures 5*c*, *d*, *f*, *g*), the secondary vortices on each side of an upstream bend of the primary vortex merge at their downstream edges and form a stronger lambda-shaped vortex that has its head symmetrically centred at and downstream of the bend of the primary vortex. Each lambda vortex resides in the braid region, and, hence, is inclined in the (x, y)-view relative to the streamwise direction.

When $\Delta\Phi = \pi$ (figure 5*e*), the flow is effectively forced by pairs of oblique waves each of equal magnitude and opposite angle without the presence of the two-dimensional excitation wavetrain. The secondary and primary vortices appear to be of equal strength, and they form (in the x, z view) a pattern of diamond-shaped cells. The streamwise length and spanwise width of each cell (measured between its edges) are λ_{KH} and λ_z, respectively. Similar structures are also apparent in numerical simulations of time-evolving compressible (Sandham & Reynolds 1991) and incompressible (Collis *et al.* 1994) mixing layers that are forced by a pair of oblique waves at the fundamental frequency. As shown in §3.3, the spanwise rows of the diamond-shaped cells are composed of adjacent pairs of spanwise vortices that are strongly deformed at the excitation wavelength λ_z in planes that are rotated around the z-axis. The deformation amplitude of each vortex is equal to or exceeds $\frac{1}{2}\lambda_{KH}$, and the cell-like appearance results from spanwise offset of the deformations of adjacent vortices by $\frac{1}{2}\lambda_z$. The passage frequency of each pair of vortices is equal to the excitation frequency and hence the number of spanwise vortices is actually doubled. These vortical structures are reminiscent of the subharmonic spanwise-localized pairing mode identified by Pierrehumbert & Widnall (1982). However, in contrast to the present observations, the subharmonic instability of Pierrehumbert & Widnall has a streamwise wavelength that

is twice that of the two-dimensional base flow. Collis *et al.* showed that when λ_z is large enough, the deformed vortices may undergo pairings at spanwise locations corresponding to streamwise edges of the diamond-shaped cells.

When $\Delta\Phi > \pi$, the secondary vortical structures weaken and again become pairs of hairpin-like counter-rotating vortices (figure 5*f–i*). Because the wavetrain in the centre segment is now leading in phase relative to its adjacent segments, the centre segment of the primary vortex is symmetrically bent around midspan in the downstream direction. The secondary vortices appear near upstream bends corresponding to the outer segments, and they are displaced in the spanwise direction by $\frac{1}{2}\lambda_z$ compared to secondary vortices resulting from phase excitation with $\Delta\Phi < \pi$. Finally, as $\Delta\Phi$ approaches 2π, the spanwise vortices become almost two-dimensional again.

The present results are compared with the observations of Browand and his coworkers (Browand & Troutt 1980, 1985; Browand & Prost-Domasky 1990) by using a time series of spanwise profiles of the streamwise velocity component to capture spanwise features of the primary vortices. For these measurements, the free-stream velocities are increased to 36 and 12 cm s^{-1}, $\nu_1 = 6.9$ Hz, $\nu_2 = 7.0$ Hz, and $\lambda_z = 7.6$ cm. The measurements are taken at equally spaced spanwise positions along $-4.5 < z < 4.5$ cm at $x = 10.2$ cm and at a y-elevation corresponding to a spanwise- and time-averaged streamwise velocity of 30 cm s^{-1}. Time series of the streamwise velocity are sampled phase-locked to the beat frequency $\nu_2 - \nu_1$ such that each data record includes 4480 samples equally spaced over the beat period. Ensemble-averaged profiles of the velocity perturbation $\langle u_{pert}(z, t)\rangle$ are calculated from 40 such data records and are shown in figure 6 during one beat period (10 s) of the two excitation wavetrains. At $t = t_0$, the flow is nominally two-dimensional but as $\Delta\Phi$ increases, the primary vortices begin to develop spanwise undulations of wavelength λ_z. (Note that, because time increases from left to right, the bend in the centre segment of the spanwise vortex points to the right.) The effect of the secondary vortices apparent in figures 5(*a, b, d, e*) is not felt at this cross-stream elevation until their strength becomes comparable with the primary vortices ($t - t_0 > 3$ s).

When $t - t_0 = 5$ s ($\Delta\Phi = \pi$), it is not possible to distinguish between the 'secondary' and 'primary' vortices, and a spanwise-cellular vortex structure emerges. The centre segment appears to be 'dislocated' (a 'vortex termination' in the parlance of Browand & Troutt 1980, 1985) from the outer segments. When $\Delta\Phi > \pi$, the secondary vortical structures weaken (as can be affirmed by their induced velocity perturbations), and the spanwise undulations of the primary vortices are essentially out of phase with respect to the undulations for $\Delta\Phi < \pi$. Although $\Delta\Phi$ varies linearly in time, the spanwise response of the flow as shown in figure 6 is not exactly symmetric in time with respect to $t - t_0 = 5$ s, for which $\Delta\Phi = \pi$. This is probably the result of a small spanwise phase distortion already present in the nominally two-dimensional base flow (cf. figure 2*b*). These data indicate that the 'dislocations' observed in the work of Browand and his coworkers are clearly connected with three-dimensional distortions of the primary vortices.

The subharmonic instability mode identified by Pierrehumbert & Widnall (1982), which can lead to spanwise-localized pairing of the primary vortices, has a short-spanwise-wavelength cutoff below which three-dimensional disturbances do not amplify. In connection with this finding, we note that whenever spanwise deformations of the primary vortices are apparent in previous experimental investigations of unforced mixing layers, the characteristic lengthscales of these deformations exceed λ_{KH}. In the present experiments, we consider the effect of λ_z on the evolution of the primary vortices for $\Delta\Phi = \pi$ (corresponding to excitation with pairs of equal and

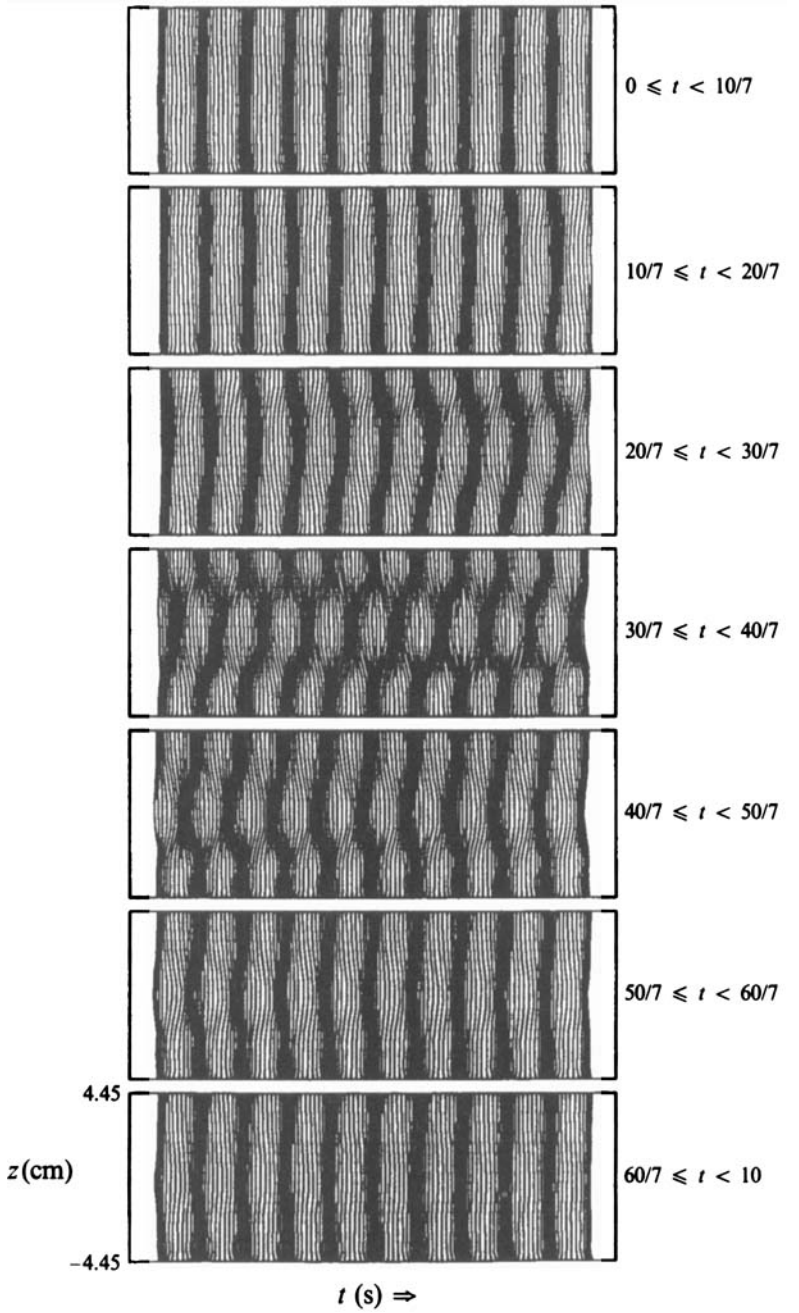

FIGURE 6. Time plots of spanwise distributions of $\langle u_{pert}(z, t)\rangle$ during the 10 s beat period of Φ_{TSP} with $\nu_1 = 6.9$ Hz, $\nu_2 = 7.0$ Hz, and $\lambda_z = 7.6$ cm. The frequency of the centre segment ($-1.9 < z < 1.9$ cm) is 6.9 Hz. The free-stream velocities are 36 and 12 cm s^{-1}, $x = 10.2$ cm, $-4.5 < z < 4.5$ cm, and the y-elevation corresponds to $U = 30$ cm s^{-1}.

opposite oblique waves only). The free-stream velocities are 30 and 10 cm s^{-1}, and the excitation frequency is 5 Hz (corresponding to $\lambda_{KH} = 4$ cm).

The response of the flow is shown in the sequence of (x, z) schlieren photographs ($1 < x < 14.2$ cm) in figure 7(*a–e*), corresponding to $\lambda_z = 6.35$, 5.08, 3.81, 2.54 and 1.27 cm, respectively. When $\lambda_z > 5.08$ cm $> \lambda_{KH}$ (figure 7*a,b*), the spanwise vortices

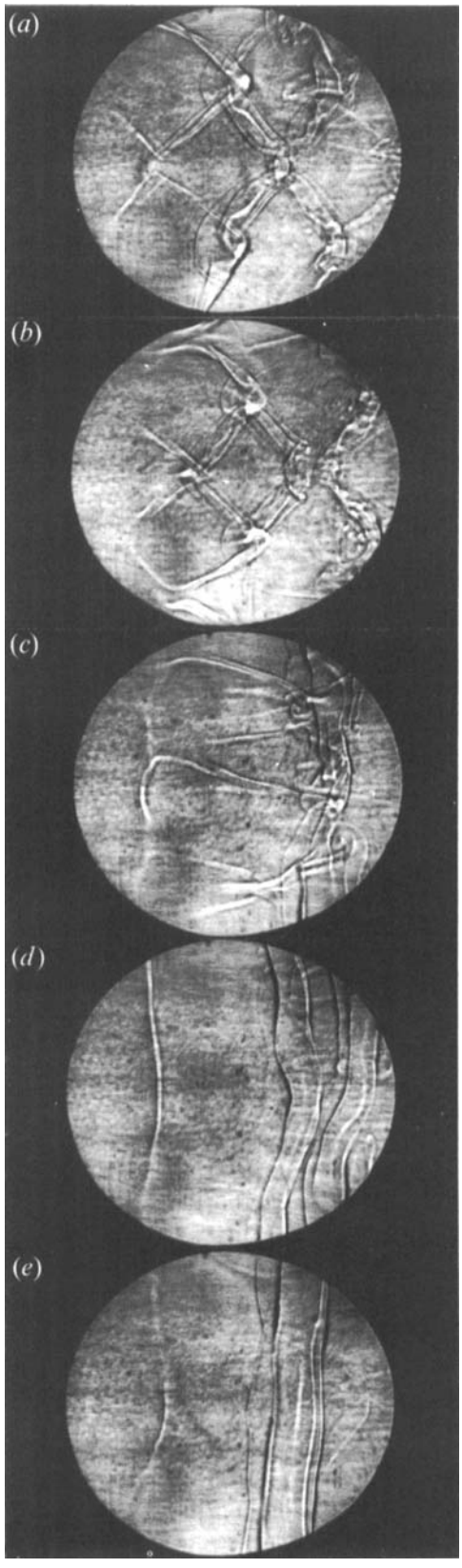

FIGURE 7. Schlieren plan (x, z) views ($3.6 < x < 16.8$ cm) showing the effect of λ_z on the evolution of the primary vortices for Φ_{SP} with $\Delta\Phi = \pi$ and $\nu = 5$ Hz. The excitation wavelengths in (*a–e*) are $\lambda_z = 6.35$, 5.08, 3.81, 2.54, and 1.27 cm, respectively.

form the diamond-shaped cells, as in figure 5(*e*). The spanwise width of each cell is approximately equal to λ_z. When $\lambda_z = 0.95\lambda_{KH}$ (figure 7*c*), the cells are replaced by pairs of lambda-shaped vortices, and spanwise distortions of the primary vortices are substantially reduced. When $\lambda_z < \lambda_{KH}$, the primary vortices become almost spanwise-uniform, and no secondary vortices appear in the braid region, indicating the existence of a short-wavelength cutoff, λ_{co}, for excitation with pairs of equal and opposite oblique waves. Although the response of the shear layer is clearly coupled to the response of the upstream boundary layer, the presence of sharp spanwise gradients in the phase-averaged distributions of streamwise velocity before the rollup of the primary vortices is completed (figure 3*c*), suggest that the cutoff results from the rollup of the shear layer. Figure 7(*c*, *d*) indicates that $\lambda_{co} \approx \lambda_{KH}$, and, since $\lambda_{KH} \approx (U_1 + U_2)/2\nu$, the corresponding cutoff spanwise wavenumber is $\beta_{co} \approx 4\pi\nu/(U_1 + U_2)$. That λ_{co} scales with λ_{KH} implies that λ_{co} increases with downstream distance and that phase disturbances of a given spanwise wavelength gradually decay as they are advected downstream.

3.3. *Excitation with pairs of equal and opposite oblique waves*

In this section, we examine in more detail some of the drastic changes in the structure of the plane mixing layer when $\Delta\Phi = \pi$ and the passage frequency of the spanwise vortices is effectively twice the excitation frequency. The overlay of upstream and downstream bends of successive spanwise vortices at the corners of the diamond-shaped cells (cf. figure 5*e*) suggests a *double rollup* of the vortex sheet that forms downstream of the flow partition. This double rollup is studied using a high-speed video movie taken at 1000 frames s^{-1}. The excitation and flow conditions are the same as in figure 5(*a–i*), where the frequencies of the centre ($-2.55 < z < 2.55$ cm) and two adjoining segments of the excitation waveform are 4.9 and 5 Hz, respectively, except that $\lambda_z = 10.2$ cm for improved resolution. Figure 8 includes a sequence of 10 video frames at 20 ms time intervals (corresponding to one period of the 5 Hz excitation waveform) centred in time around $\Delta\Phi = \pi$ (i.e. during this sequence $\Delta\Phi$ changes between 0.98π and 1.02π).

In figure 8(*a*), the rollup of the centre segment of the primary vortex CS_1, which is forced at 4.9 Hz, is just beginning on the left-hand side. The centre segment of the primary vortex that rolled up in the previous cycle of the excitation waveform, CS_2, is λ_{KH} downstream from CS_1 and appears to bifurcate symmetrically about midspan into upstream and downstream oblique branches, each connected to the 'outer' segments of the primary vortices at the upper and lower edges of the photograph. The segments OS on each side of midspan are (approximately) $\frac{1}{2}\lambda_{KH}$ upstream and downstream relative to CS_2. As the rollup of CS_1 continues (figure 8*b–d*), there is also a rollup of an oblique upstream branch of each of the segments OS. As shown in §3.4, each of these branches loops above a neighbouring downstream branch of OS and is stretched toward CS_1 (marked by an arrow in figure 8*c*). In figure 8(*e*), each of the upstream branches appears to be connected to CS_1 (ostensibly close to the low-speed side owing to the velocity field induced by CS_1). In figure 8(*f*), upstream branches begin to roll up at each spanwise edge of CS_1 and near the top and bottom of the frames in figure 8(*f*, *g*) (recall that these OS form approximately half the excitation period after CS_1).

Figure 8(*g*, *h*) indicates that the rollup of the upstream and downstream branches at each spanwise edge of CS_1 continues and, as a result, CS_2 in figure 8(*b–d*) separates into two distinct vortical cores. The evolution of these cores is further confirmed by dye visualization (figure 9*b*), where the dye is injected at midspan of the low-speed boundary layer and thus through the centre of CS_1 in the (x, y) plan view. (Figure 9*a*

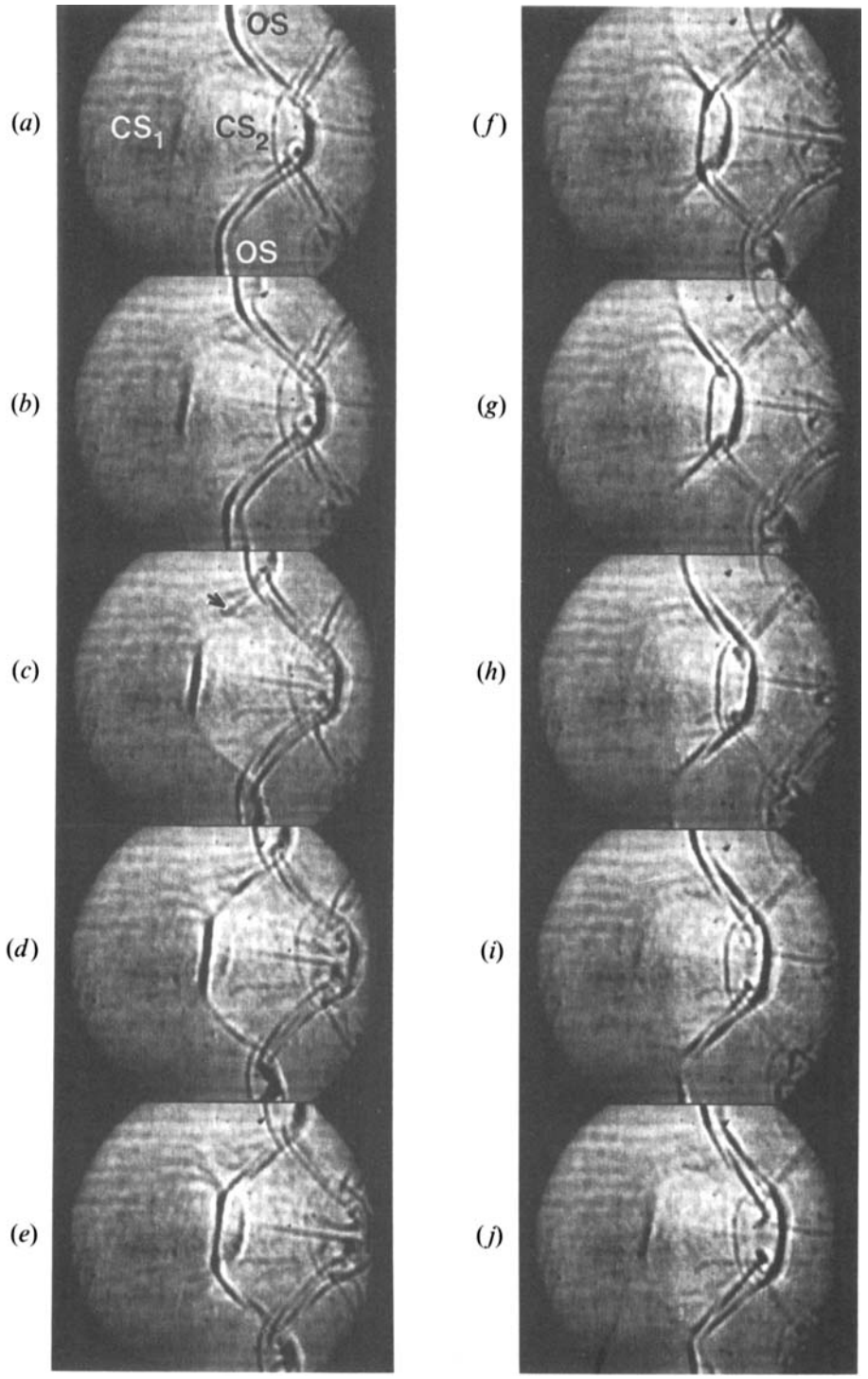

FIGURE 8. Ten frames from a high-speed (1000 frames s^{-1}) schlieren movie (in the x, z-plane). The excitation and flow conditions are the same as in figure 5(*a–i*) (except that $\lambda_z = 10.2$ cm). The frequencies of the centre ($-2.55 < z < 2.55$ cm) and the two adjoining segments of the excitation waveform are 4.9 and 5 Hz, respectively. The frames (*a–j*) are taken 20 ms apart and are centred in time around $\Delta\Phi = \pi$.

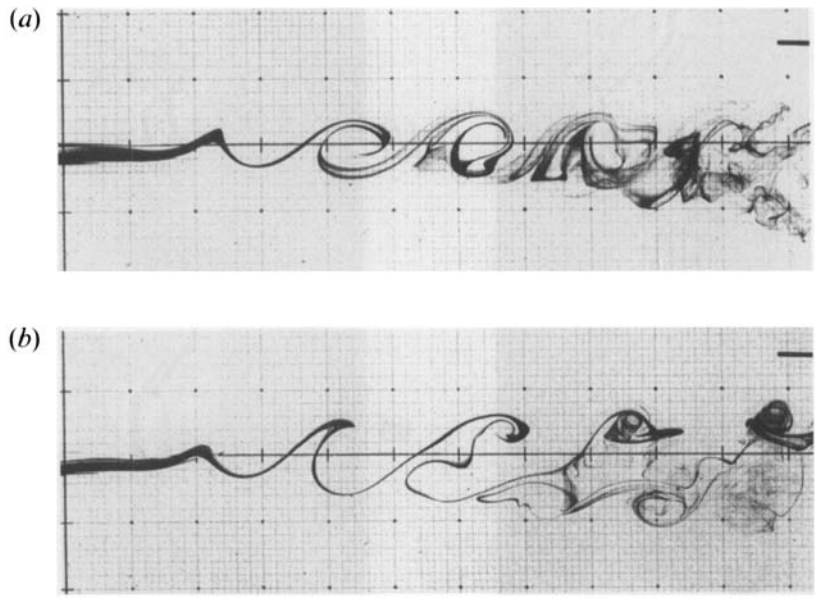

FIGURE 9. Dye (injected at midspan) visualization in the cross-stream (x, y)-plane: (*a*) spanwise-uniform excitation; (*b*) $\Delta\Phi = \pi$ ($\lambda_z = 5.1$ cm) showing the double rollup of the spanwise vortices. The grid in (*a*) and (*b*) is square and measures 2.54 cm on the side. The vertical axis is at $x = 0$.

corresponds to spanwise-uniform excitation and is shown for reference.) Because adjacent segments of the excitation waveform have almost the same frequency and presumably the same streamwise amplification, the double rollup of each spanwise segment begins at the same distance downstream from the flow partition. However, since adjacent segments of the excitation waveform are out of phase (i.e. $\Delta\Phi = \pi$), the double rollup alternates at twice the excitation frequency between segments centred at $z = \pm j\lambda_z$ and at $z = \pm(j\lambda_z + \frac{1}{2}\lambda_z)$ $(j = 0, 1, 2, \ldots)$. In figure 5(*e*), the double rollup occurs at each corner of the diamond-shaped cells, thus leading to the formation of two separate spanwise-undulated vortices during each period of the excitation waveform. These vortices are undulated in planes that are tilted around the z-axis relative to the streamwise direction so that their downstream bends are at higher cross-stream elevations than their upstream bends. Each pair of adjacent vortices is offset in the z-direction by $\frac{1}{2}\lambda_z$, and thus CS_2 in figure 8(*c*) and the corners of the diamond-shaped cells in figure 5(*e*) are overlays of downstream and upstream edges of the undulated vortices.

Some features of the flow when $\Delta\Phi = \frac{1}{2}\pi$ and π (figures 10*a* and 10*b*, respectively) are studied using cross-stream distributions of the streamwise velocity component measured at a number of equally spaced streamwise stations at $z_1 = 0$, $z_2 = z_1 + \frac{1}{4}\lambda_z$, and $z_3 = z_1 + \frac{1}{2}\lambda_z$. These measurements are taken when the excitation frequency is 5 Hz and spanwise-uniform ($\lambda_{KH} \approx 4$ cm) and the (time-invariant) spanwise phase programme is Φ_{SP} with $\lambda_z = 5.1$ cm. Similar to figures 5(*a–i*) and 8(*a–j*), $\Phi(z)$ is symmetric about $z = 0$, and the phase discontinuity occurs at z_2. In fact, comparison of figure 10(*a*, *b*) with figure 5(*a–i*) shows that the structure of the shear layer for phase programmes Φ_{SP} and Φ_{TSP} is virtually the same for a given $\Delta\Phi$ even though the cross-stream circulation of the primary vortices varies slightly across frequency discontinuities of the excitation waveform. While $\Delta\Phi$ for figure 10(*a*) falls between $\Delta\Phi$ of figures 5(*c*) and 5(*d*), the similarity between figures 10(*b*) and 5(*e*) is clearly apparent.

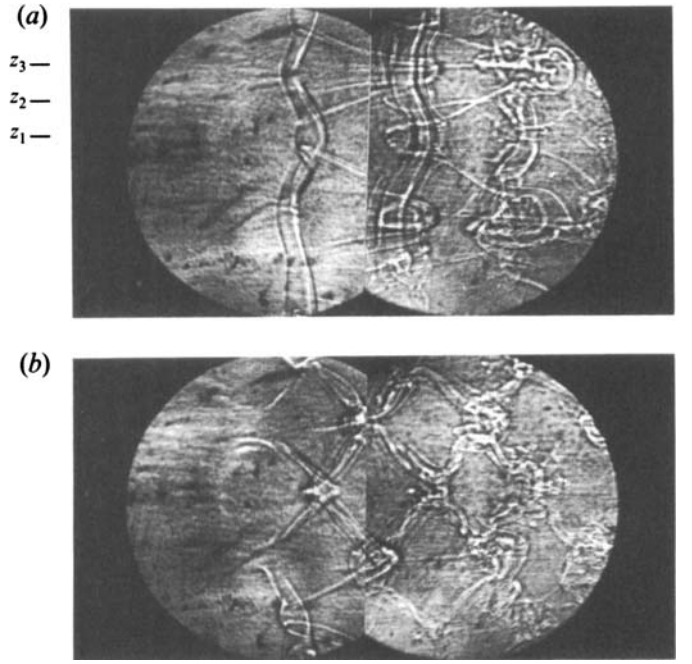

FIGURE 10. Schlieren plan (x, z) views showing the effect of phase programme Φ_{SP} with $\nu = 5.0$ Hz, $\lambda_z = 5.1$ cm, and $\Delta\Phi = \frac{1}{2}\pi$ (a), and π (b) (z_1, z_2, and z_3 are spanwise measurement stations).

Figure 11(a, b) shows perspective contour plots of phase-averaged turbulent fluctuations, $\langle u'_{trms}(y, t)\rangle$ (computed relative to the pseudo-mean instantaneous velocity (Glezer, Katz & Wygnanski 1989)), measured at z_1, z_2, and z_3 at $x = 15.2$ cm during two periods of the excitation wavetrain. When the excitation waveform is spanwise-uniform (figure 11a, $z = z_1$), passage of the spanwise vortices at the measurement station can be recognized by concentrations of small-scale velocity fluctuations. At this streamwise position, the cross-stream distribution of $\langle u'_{trms}\rangle$ within the spanwise vortex exhibits a fairly broad peak near the low-speed side.

When $\Delta\Phi = \pi$ (figure 11b), the planes $z = z_1$ and z_3 are (y, t) cross-sections through successive streamwise corners of the diamond-shaped cells in the (x, y) plan view of figure 5(e), while the plane $z = z_2$ is a (y, t) cross-section through the sides of these cells halfway between z_1 and z_3. Concentrations of $\langle u'_{trms}\rangle$ in the planes $z = z_1$ and z_3 are reasonably similar and are offset in time by half the excitation period. While y-elevations of the centres of the vortical structures in the planes $z = z_1$ and z_3 alternate in time between the high- and low-speed sides of the shear layer, the centres of successive cross-sections in the plane $z = z_2$ have approximately the same y-elevations. Figure 11(b) also shows that concentrations of $\langle u'_{trms}\rangle$ in each of the (y, t)-planes appear twice during each excitation cycle, reaffirming the observation that, when $\Delta\Phi = \pi$, there is a double rollup of the spanwise vortices. The centres of the cores of the spanwise vortices are outlined by dashed lines, showing the overlay of upstream and downstream bends of successive spanwise vortices at $x = z_1$ and z_3.

The streamwise amplifications of velocity perturbations at the forcing frequency and its first harmonic are determined from distributions of their cross-stream integrated amplitudes, $A_1(x, z)$ and $A_2(x, z)$, respectively, without further decomposition into spanwise modes. Figure 12(a) shows A_1 (closed symbols) and A_2 (open symbols) for

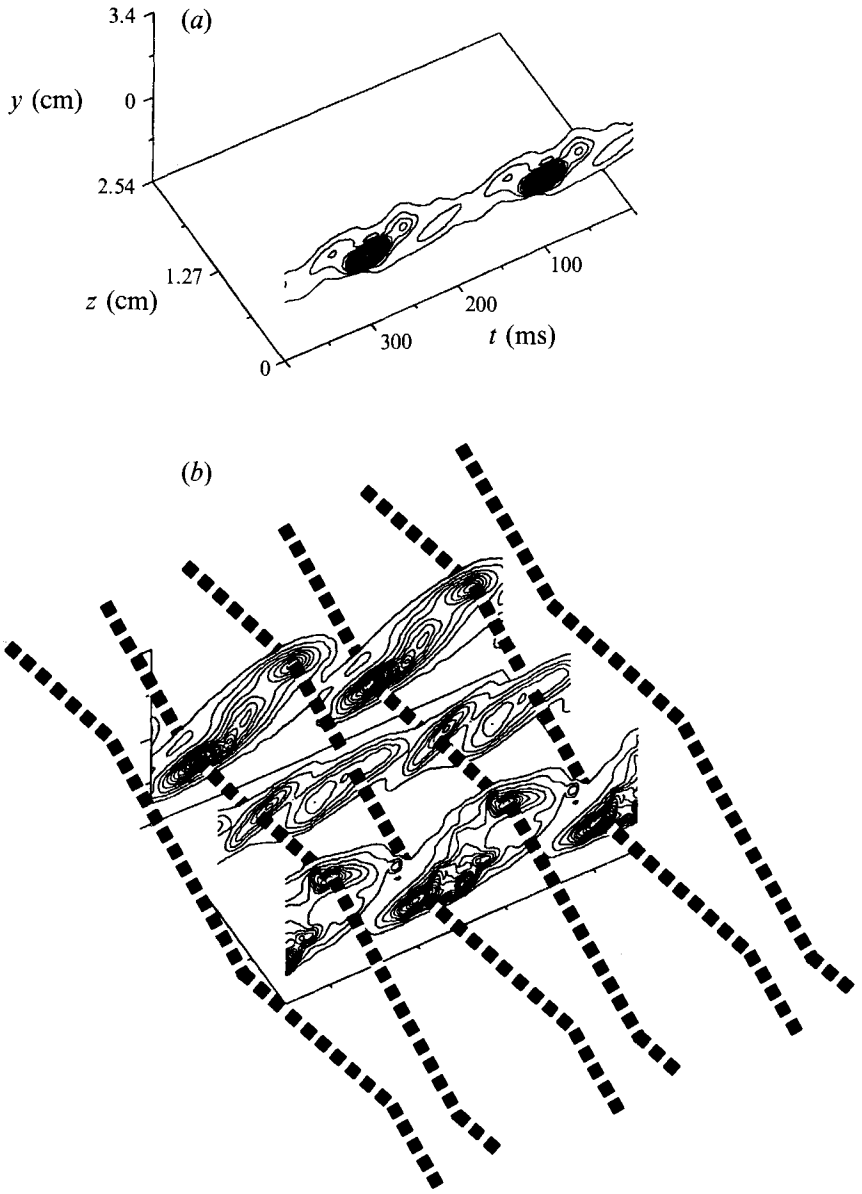

FIGURE 11. Perspective contour plots of $\langle u'_{trms}(y,t)\rangle$, measured at z_1, z_2, and z_3 (cf. figure 10*a*) at $x = 15.2$ cm during two periods of the excitation wavetrain: (*a*) Φ_{SU} (at $z = z_1$); (*b*) Φ_{SP} with $\Delta\Phi = \pi$ (the centres of the cores of the spanwise vortices are outlined by dashed lines showing the overlay of upstream and downstream bends of successive spanwise vortices at z_1 and z_3). Contours start at 0.25 cm s^{-1}, with contour increments of 0.25 cm s^{-1}.

$\Delta\Phi = 0$ (spanwise-uniform excitation), $\frac{1}{2}\pi$, and π. Figure 12(*b*) shows corresponding distributions of the momentum thickness

$$\theta(x,z) = \frac{1}{\Delta U^2}\int_{-\infty}^{\infty} |[U(x)-U_2][U_1-U(x)]|\,\mathrm{d}y,$$

where $\Delta U = \frac{1}{2}(U_1+U_2)$ and the absolute value of the integrand is used to prevent artificial reduction in the magnitude of the momentum thickness due to distortions of the mean velocity profile $U(x)$. In figures 12(*a*) and (*b*), the data corresponding to spanwise-uniform excitation were obtained at $z = z_1$ and are replotted at $z = z_2$ and z_3

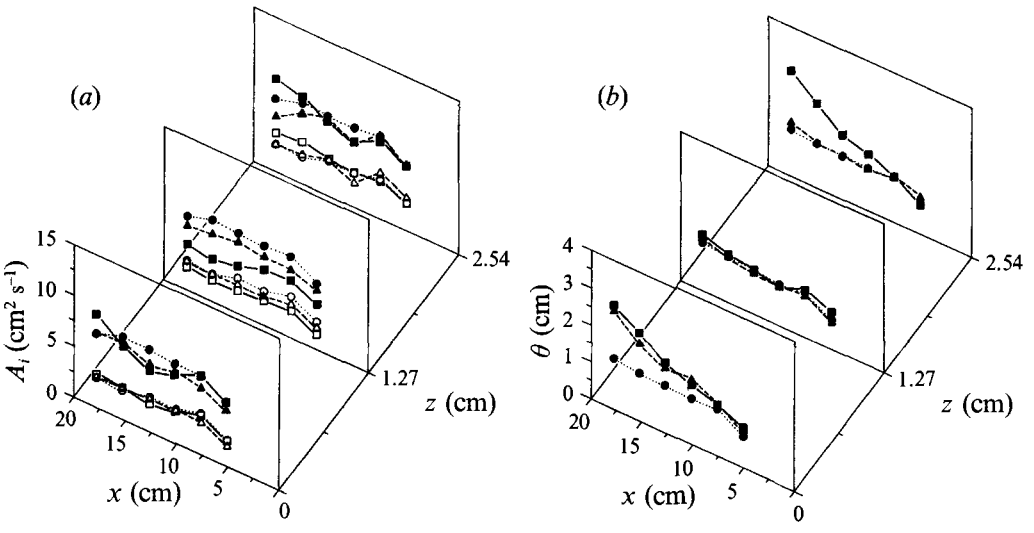

FIGURE 12. Streamwise distributions at z_1, z_2, and z_3 of (*a*) cross-stream integrated amplitudes $A_1(x, y)$ (closed symbols) and $A_2(x, z)$ (open symbols) of $u_{pert}(z, t)$ at ν and 2ν; and (*b*) $\theta(x, z)$: Φ_{SU} (circles); Φ_{SP} with $\Delta\Phi = \frac{1}{2}\pi$ (triangles), and $\Delta\Phi = \pi$ (squares).

for reference. When $\Delta\Phi = 0$, A_1 and θ increase somewhat between $x = 5.1$ and 7.6 cm and then remain almost unchanged through $x = 15.2$ cm, where A_1 begins to decay.

Streamwise distributions of A_1 and θ at $z = z_1$ and z_3 for $\Delta\Phi = \pi$ are quite similar because, apart from a phase shift, the flow is virtually identical at these cross-stream planes. The distributions of A_1 at $z = z_1$ and z_3 indicate that the perturbation wavetrain is amplified for $x < 7.5$ cm, followed by saturation at $x \approx 7.5$ cm and a slight decay for $7.5 < x < 15$ cm (where the double rollup occurs). The amplification of the wavetrain at the fundamental frequency continues for $x > 15$ cm through to the end of the streamwise domain considered here. The momentum thickness of the forced flow at $z = z_1$ and z_3 is substantially larger than the momentum thickness of the unforced flow. Although the streamwise rate of increase of $\theta(x, z)$ diminishes slightly for $10 < x < 15$ cm, at $x = 17.8$ cm, the momentum thickness of the forced flow at $z = z_1$ and z_3 (and hence at $z = \pm j\lambda_z/2$ ($j = 0, 1, 2, \ldots$)) is approximately 120% greater than for $\Delta\Phi = 0$. At $z = z_2$, the excitation wavetrain has a local minimum, and $A_1(x)$ and $\theta(x)$ are quite different from the corresponding distributions at z_1 and z_3. While A_1 is amplified for $x < 7.6$ cm and then undergoes saturation (at $x \approx 10.2$ cm) followed by attenuation, θ exhibits a small decrease at $x \approx 10.2$ cm followed by a small increase for $x > 10.2$ cm. It is remarkable that, at $z = z_2$, $\theta(x)$ for $\Delta\Phi = 0$ and π are almost identical for $x > 10$ cm.

In contrast to the case $\Delta\Phi = \pi$, there is considerable disparity between respective streamwise distributions of A_1 and θ at $z = z_1$ and z_3 when $\Delta\Phi = \frac{1}{2}\pi$. This disparity is noteworthy because the frequencies of adjacent segments of the excitation waveform and, presumably, their streamwise amplifications are approximately the same. The differences between $A_1(x)$ at $z = z_1$ and z_3 are apparently related to the different y-elevations of the cores of the spanwise vortices at these (x, y)-planes. Recall that, when $\Delta\Phi < \pi$, the spanwise vortices are undulated in planes that are tilted around the z-axis relative to the flow direction. Hence, (x, y) sections through downstream (at $z = z_1$) and upstream (at $z = z_3$) bends of these vortices are closer to the high- and low-speed edges of the shear layer, respectively. At $z = z_2$, the cores of the primary vortices are not significantly displaced in the cross-stream direction relative to the case of spanwise-uniform excitation, and the streamwise amplification of the excitation wavetrain is

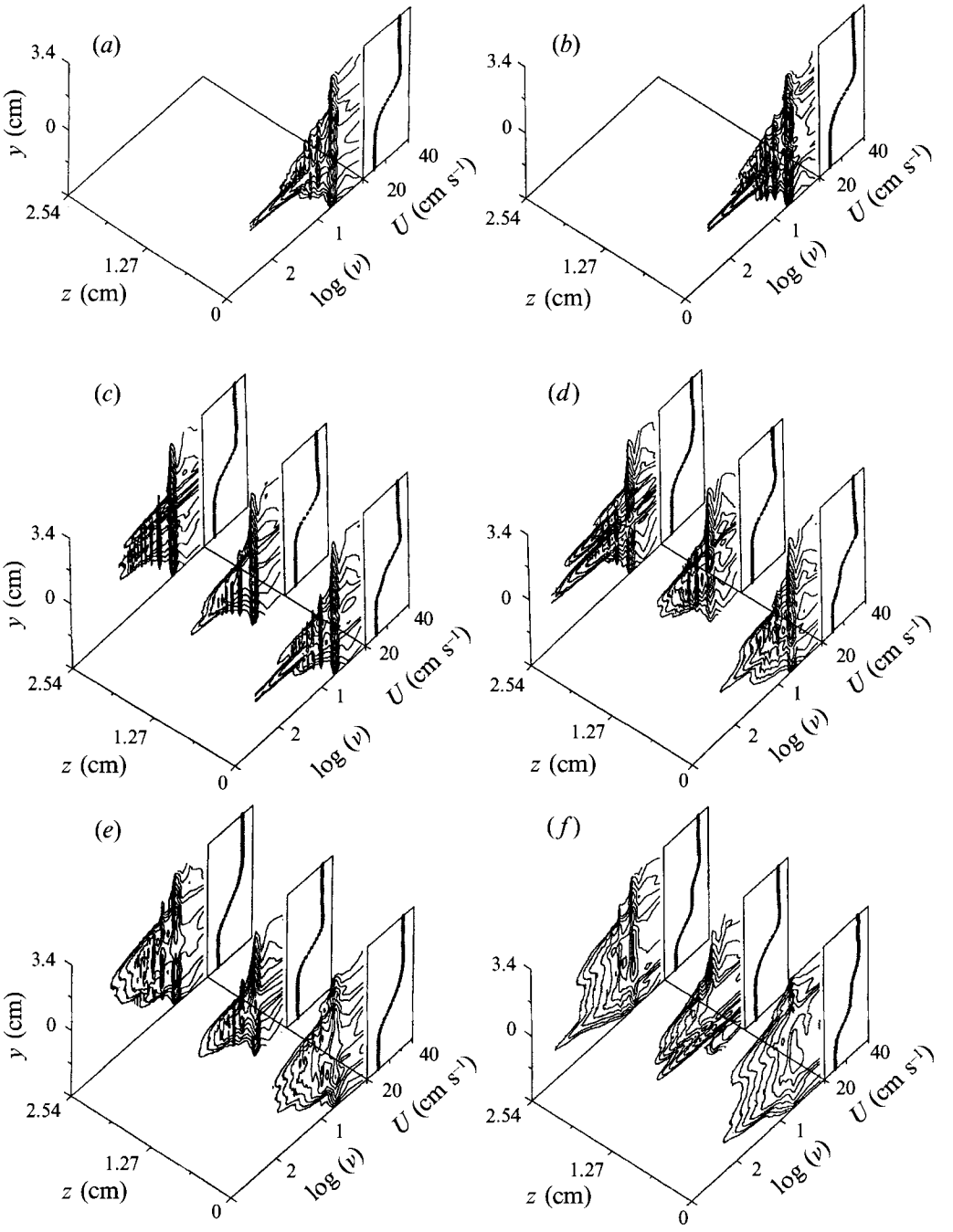

FIGURE 13. Composites of cross-stream contour plots of $P(\nu, y)$ and profiles of $U(y, x)$ measured at z_1, z_2, and z_3 at $x = 10.2$ (*a*, *c*, and *e*), and 15.2 cm (*b*, *d*, and *f*): Φ_{SU} at z_1 (*a*, *b*); Φ_{SP} with $\Delta\Phi = \frac{1}{2}\pi$ (*c*, *d*) and with $\Delta\Phi = \pi$ (*e*, *f*). Contour increments are logarithmic, starting at 10^{-3} cm^2 s^{-2}, and the ratio of consecutive contours is $10^{0.5}$.

qualitatively similar to that of the two-dimensional wavetrain even though the levels of A_1 at corresponding streamwise stations are higher for the latter. While the distributions of $\theta(x)$ for $\Delta\Phi = 0$ and $\frac{1}{2}\pi$ are almost identical at $z = z_2$ and z_3, at $z = z_1$, $\theta(x)$ for $\Delta\Phi = \frac{1}{2}\pi$ is closer to $\theta(x)$ for $\Delta\Phi = \pi$. This indicates that distortions of $U(y, x)$ near the low-speed side (associated with upstream bends of the primary vortices) have a smaller effect on $\theta(x)$ than corresponding distortions near the high-speed side (associated with downstream bends of the primary vortices). Even though a direct comparison of momentum thickness for $\Delta\Phi = \frac{1}{2}\pi$ and π between the present experiments and the simulations of Collis *et al.* is not possible because the numerical data are spanwise-averaged, there is a qualitative agreement between their results and the distributions of $\theta(x)$ at $z = z_3$.

Composites of cross-stream contours of power spectra, $P(\nu, y)$, and profiles of $U(y, x)$ at $z = z_1$, z_2, and z_3 are shown for $x = 10.2$ and 15.2 cm, respectively in figure 13(*a*, *b*) (spanwise-uniform excitation, measured at z_1 only), figure 13(*c*, *d*) ($\Delta\Phi = \frac{1}{2}\pi$), and figure 13(*e*, *f*) ($\Delta\Phi = \pi$). When the excitation waveform is spanwise uniform, the distributions of $P(\nu, y)$ have pronounced peaks at the excitation frequency and some of its higher harmonics and do not vary substantially between $x = 10.2$ and 15.2 cm. A cross-stream band of high-frequency spectral components near the low-speed edge of the mixing layer is associated with the presence of small-scale motion and corresponds to concentrations of $\langle u'_{trms} \rangle$ in figure 11(*a*).

When the flow is forced with $\Delta\Phi = \frac{1}{2}\pi$ (figure 13*c*, *d*) and π (figure 13*d*, *e*), the evolution of the secondary vortical structures is accompanied by the appearance of small-scale motion near cross-stream distortions of $U(y)$ at the high- and low-speed edges of the shear layer (cf. N&G). For $\Delta\Phi = \frac{1}{2}\pi$ (figure 13*c*, *d*) this is evidenced by bands of spectral components at higher frequencies near the high- and low-speed edges at z_3 (the head) and z_1 (the tail), respectively. When $\Delta\Phi = \pi$ (figure 13*e*, *f*), the cross-stream width of the mixing layer increases considerably (particularly at $z = z_1$ and z_3) with a corresponding spreading in cross-stream concentrations of high-frequency spectral components. A noteworthy feature of $P(\nu, y)$ at $x = 15.2$ cm (figure 13*f*) is the two broad bands near the high- and low-speed edges of the layer that are consistent with the double rollup of the shear layer into pairs of vortices of the same sign and (presumably) of equal strength. The substantial increase in cross-stream concentrations of small-scale motion when $\Delta\Phi = \frac{1}{2}\pi$ and π indicates that phase excitation can lead to mixing enhancement. In fact, the simulations of Collis *et al.* show that the spanwise-averaged mixedness in substantially increased from $\Delta\Phi = \frac{1}{2}\pi$ to $\Delta\Phi = \pi$.

3.4. *Spanwise-isolated phase discontinuity*

The spanwise symmetry of the secondary vortices in §3.2 (e.g. figure 5*c*, *d*) is associated with the spanwise-periodicity of the excitation waveform. In this section, we focus attention on the evolution of an *isolated* step discontinuity in the phase of the excitation waveform in the absence of adjacent discontinuities. A spanwise step change in phase leads to a localized distortion of the primary vortices and a concomitant formation of secondary vortex strands. Unlike a spanwise-isolated amplitude perturbation (as may be effected by a 'point' disturbance on the flow partition), a spanwise phase discontinuity can result in a *single* clockwise or counterclockwise secondary vortex strand that lacks the symmetry of the lambda vortices discussed in §3.2. In what follows, the phase discontinuity occurs at midspan ($z = 0$) between two spanwise-uniform segments of $E(z, t)$. As in §3.2, the frequencies of adjacent segments are 5 Hz (for $z < 0$) and 4.9 Hz (for $z > 0$), and $\Delta\Phi$ is measured relative to the segment $z < 0$. Figure 14(*a–g*) is a sequence of (x, z) schlieren photographs

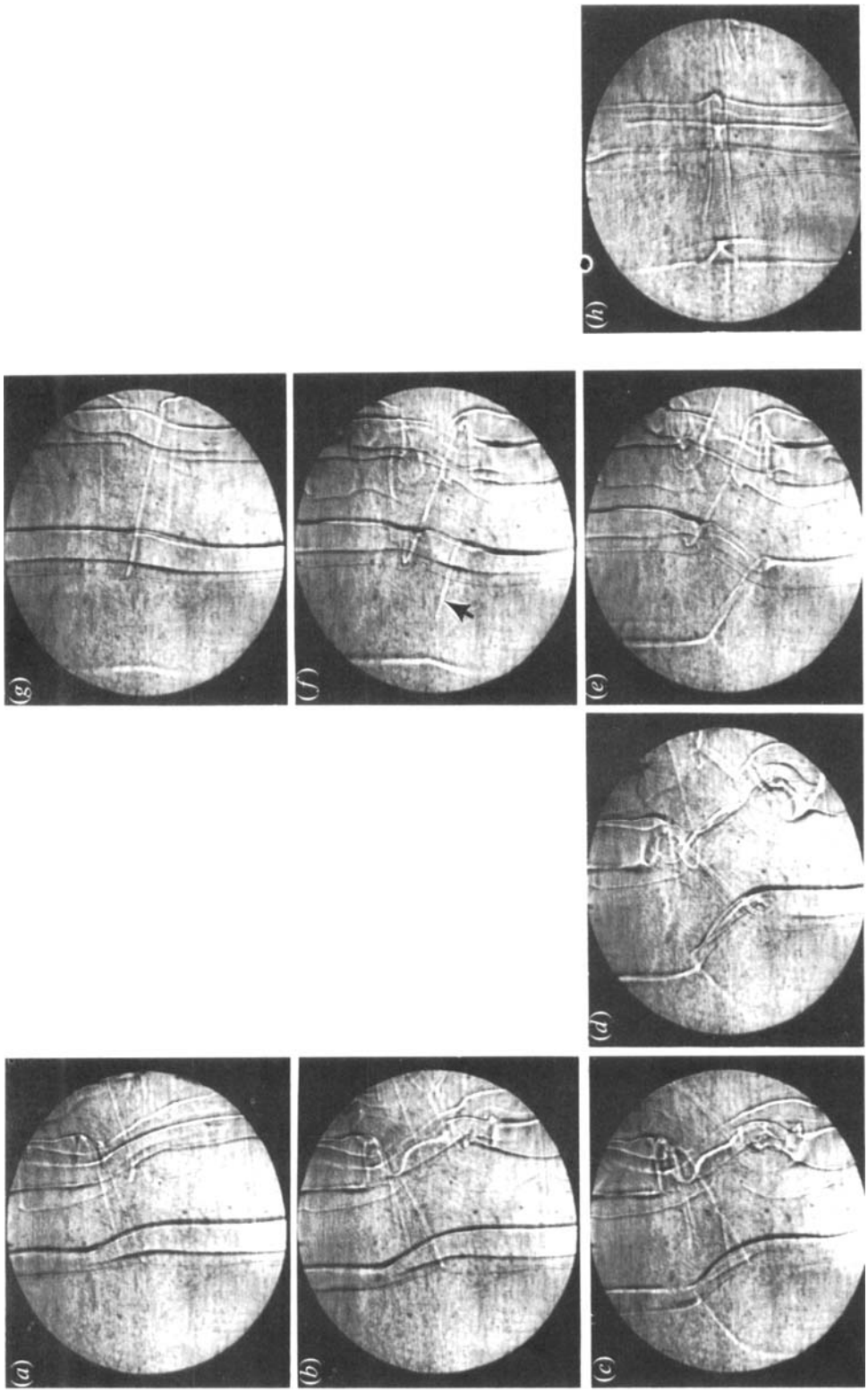

FIGURE 14. Schlieren plan (x, z) views ($3.6 < x < 16.8$ cm) showing the evolution of isolated phase (a–g) and amplitude (h) discontinuities at midspan ($z = 0$). In (a–g) the phase programme is Φ_{sp} with $\nu_1 = 5$ Hz (for $z < 0$) and $\nu_2 = 4.9$ Hz (for $z > 0$). Frames (a–g) were taken phase-locked to the beat frequency $\nu_2 - \nu_1$ at 1 s time intervals ($\Delta\Phi = \pi$ in d). In (h), $\Phi(z)$ = constant and $E_0(z)$ has a step discontinuity at midspan.

($3.6 < x < 16.8$ cm) that are taken under the same conditions as in figure 5(*b–h*), respectively ($\Delta\Phi = \pi$ in figure 14*d*). In figure 14(*h*) the excitation waveform has no spanwise phase or frequency variations but there is a step discontinuity in amplitude at midspan. This figure is included for reference and will be discussed further below.

In figure 14(*a–c*) ($\Delta\Phi = 0.4\pi$, 0.6π and 0.8π, respectively), $E(z > 0, t)$ lags in phase relative to $E(z < 0, t)$. In figure 14(*e–g*) ($\Delta\Phi = 1.2\pi$, 1.4π and 1.6π, respectively), $E(z > 0, t)$ leads in phase relative to $E(z < 0, t)$. As a result, adjacent spanwise segments of the primary vortices become distorted near midspan due to spanwise-non-uniform rollup. For $\Delta\Phi < \pi$ (or $\Delta\Phi > \pi$), rollup of the segments $z < 0$ (or $z > 0$) of the primary vortices occurs before rollup of the adjacent segments $z > 0$ (or $z < 0$). For example, figure 14(*f*) ($\Delta\Phi = 1.4\pi$) shows an incomplete rollup on the left-hand side. Near the phase discontinuity ($z = 0$), the primary vortices develop an upstream bend and become almost antisymmetric about midspan (there is a slight spanwise offset in figure 14*a, b*). The most noteworthy features in figure 14(*a–g*) are the nearly oblique segments of the deformed primary vortices and the appearance of secondary vortices in the braid region between these segments. The length of the oblique segment L and the angle between its axis and the z-axis (using the notation of figure 4*a*) increase with $\Delta\Phi$ and reach a maximum when $\Delta\Phi = \pi$ ($L \approx 1.2\lambda_{KH}$ and $\psi \approx \frac{1}{4}\pi$).

The spanwise projection of each oblique segment, which is a measure of the domain of influence of the spanwise discontinuity of the excitation waveform, increases only slightly with $\Delta\Phi$ and is approximately equal to $0.88\lambda_{KH}$ for $\Delta\Phi = \pi$. By comparison, measurements of the streamwise velocity perturbations for $\Delta\Phi = \pi$ (figure 3*c*) indicate that, before the rollup of the primary vortices is completed, the spanwise spreading of the disturbance resulting from the phase discontinuity is smaller than $0.2\lambda_{KH}$. The apparent increase in the width of the spanwise domain, which is affected by the phase discontinuity as the rollup of the primary vortex progresses, is connected with the limitation on the local curvature of its core (or the minimum bending radius) at the upstream and downstream edges of the oblique segment. This radius clearly scales with the local shear-layer vorticity thickness (or the core diameter of the primary vortices). As can be seen in figure 14(*a–g*) when $\Delta\Phi$ increases, this radius decreases along with the core diameter of the oblique segment of the primary vortex. When $\Delta\Phi = \pi$, the core diameter of each vortex branch near midspan is smaller than the core diameter of the undisturbed primary vortex.

The distortion of the primary vortices is accompanied by the formation of secondary vortices in the braid region between the oblique segments and the degree of inclination of the secondary vortices relative to the x-axis depends on the magnitude of $\Delta\Phi$. (Note the symmetry between figures 14*a* and 14*g*, 14*b* and 14*f*, and 14*c* and 14*e*.) The rollup of the secondary vortices begins near an upstream bend of a primary vortex (at the high-speed edge) and continues through the braid region toward the downstream bend of the subsequent primary vortex (at the low-speed edge). This is demonstrated in figure 14(*f*) which shows a partially rolled-up secondary vortex (marked with an arrow). The apparent 'termination' of this vortex strand is caused by the fact that planar vortex sheets (marked with slightly heated fluid) are not visualized by the schlieren system.

When $\Delta\Phi$ is small, the secondary vortices are lambda-shaped counter-rotating vortex pairs. Figure 14(*a*) shows such a pair where the upper leg (in the x, z-view) is rotating counterclockwise and the lower leg is rotating clockwise when viewed in the (x, z)-plane in the streamwise direction. As $\Delta\Phi$ increases, the oblique segments of the primary vortices induce a localized secondary shear flow in the braid region (in the negative $\tilde{z}$-direction of figure 4*a*), which is 'favourable' to the clockwise leg and

'adverse' to the counterclockwise leg. As a result, the counterclockwise leg is weaker and, in figure 14(*c*), it almost disappears. At the same time, the clockwise leg becomes stronger and, when $\Delta\Phi = \pi$, it is almost indistinguishable from the oblique segment of the primary vortex. Similarly, in figure 14(*e*, *f*), the induced secondary shear layer in the braid region has a velocity component in the positive $\tilde{z}$-direction (figure 4*a*). As $\Delta\Phi$ increases further (figure 14*e*), the lower (clockwise) vortex leg becomes weaker and disappears from the braid region and the counterclockwise segment becomes stronger. The sense of rotation of the remaining legs of the secondary vortices in the braid region (i.e. clockwise when $\Delta\Phi < \pi$ and counterclockwise when $\Delta\Phi > \pi$) was verified using high-speed video photography and is shown schematically in figure 15(*a*, *b*).

As $\Delta\Phi$ approaches π (figure 14*d*), the secondary vortices and the oblique segments of the primary vortices appear to be of equal strength. (We note that when $\Delta\Phi$ is time-invariant in an unbounded flow, the circulation over λ_{KH} in the (x, y)-plane $z = 0$ must be the same as in (x, y)-planes on both sides of the phase discontinuity.) Each segment of a primary vortex below (or above) midspan bifurcates into a pair of upstream and downstream branches of approximately equal length. These branches are connected below (or above) midspan to neighbouring segments of the primary vortices $0.5\lambda_{KH}$ in the upstream and downstream directions (shown schematically in figure 15*c*). Flow visualization indicates that, in the (x, z) plan view of a pair of branches, the upstream branch loops above the downstream branch while the centres of the primary vortices above and below midspan remain at the same cross-stream elevation (figure 15*c*). Figure 14(*f*) further suggests that the vortex bifurcation is not stable and continues along the axes of the spanwise vortices. In fact, when the phase programme is Φ_{TSP} and $\Delta\Phi < \pi$ (or $> \pi$) (e.g. figure 5), strong lambda-shaped vortices are formed through the merging of adjacent counter-rotating pairs of secondary vortex strands each induced by a phase discontinuity of the excitation wavetrain. Recent dye-visualization studies in a plane shear layer (Nassef & Browand 1993) and some measurements in a cylinder wake (Williamson 1992) indicate that such bifurcations are accompanied by spanwise flow along the axes of the primary vortices.

Previous experimental work (e.g. Lasheras *et al.* 1986) has shown that an isolated (point) disturbance in the flow partition's boundary layer results in the formation of secondary lambda-shaped counter-rotating vortex pairs in the 'braid' region between primary vortices. These disturbances can be synthesized by spanwise variations in the amplitude of a time-harmonic excitation having spanwise-uniform phase and frequency distributions (N&G). As shown above, the secondary vortices resulting from a phase discontinuity when $\Delta\Phi$ is small, are very similar to the lambda-shaped vortices studied by N&G. However, when $\Delta\Phi$ is large enough, each secondary vortex pair evolves into a single vortex due to the secondary shear flow in the braid region. To amplify this point, the flow conditions in the (x, z)-view in figure 14(*h*) are the same as in figure 14(*a–g*), but the amplitude of the excitation waveform is piecewise-constant with a spanwise discontinuity at midspan and with no spanwise variations in phase or frequency. Unlike the phase discontinuity in figure 14(*a–g*), an amplitude discontinuity of the excitation waveform results in the formation of a single secondary lambda-shaped vortex, without an appreciable deformation of the primary vortex.

3.5. *The effect of phase distortion on the secondary vortices*

The experiments of N&G have shown that time-harmonic excitation with a spanwise-periodic amplitude distribution E_{SP}, leads to the formation of secondary counter-rotating vortex pairs having spanwise spacings that are equal to the excitation wavelength, λ_z. The included angle Λ between the legs of these lambda-shaped vortices

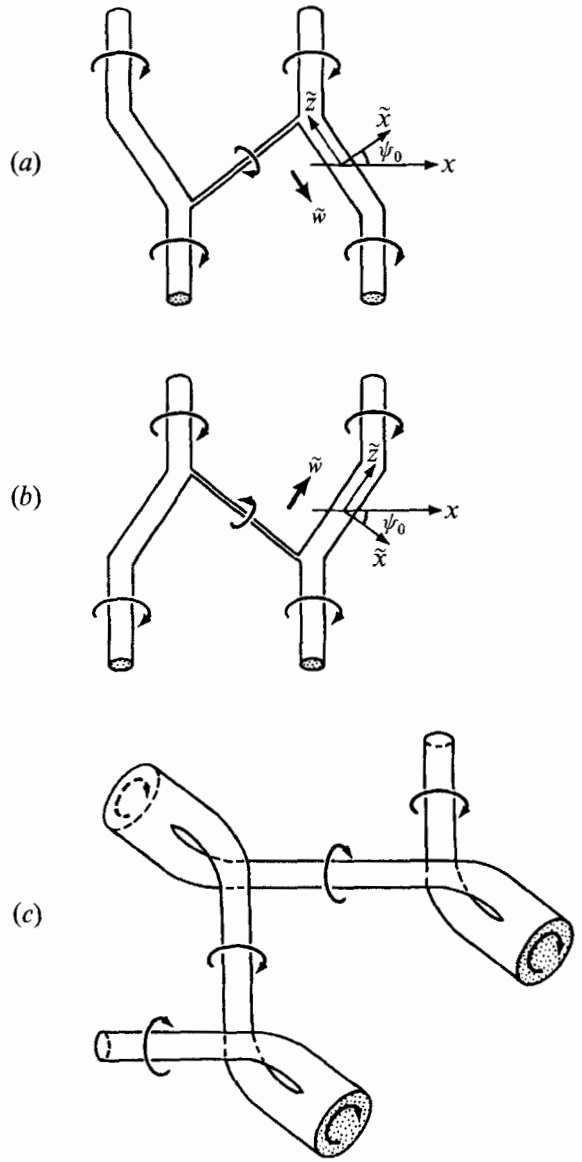

FIGURE 15. Schematic drawings of vortex connections when $\Delta\Phi < \pi$ (*a*), $\Delta\Phi > \pi$ (*b*), and $\Delta\Phi = \pi$ (*c*).

decreases with decreasing λ_z, and they can be formed at virtually any spanwise wavelength synthesizable by the heating mosaic. N&G noted that, when $\lambda_z > \lambda_{KH}$, the primary vortices develop spanwise deformations at the excitation wavelength (e.g. figure 16*a* where $\lambda_z = 5.1$ cm and $\nu = 5$ Hz). These deformations are considerably less apparent when $\lambda_z < \lambda_{KH}$. Because the phase of the excitation wavetrain is spanwise uniform, it appears that the phase distortion that leads to upstream bends of the primary vortices (figure 16*a*) is induced by the formation of the streamwise vortices *upstream* of the first rollup of the primary vortices. The subsequent spanwise modifications of the strain field in the braid region between adjacent primary vortices result in an increase in A farther downstream and in the appearance of additional secondary vortices on each side of the original secondary vortex.

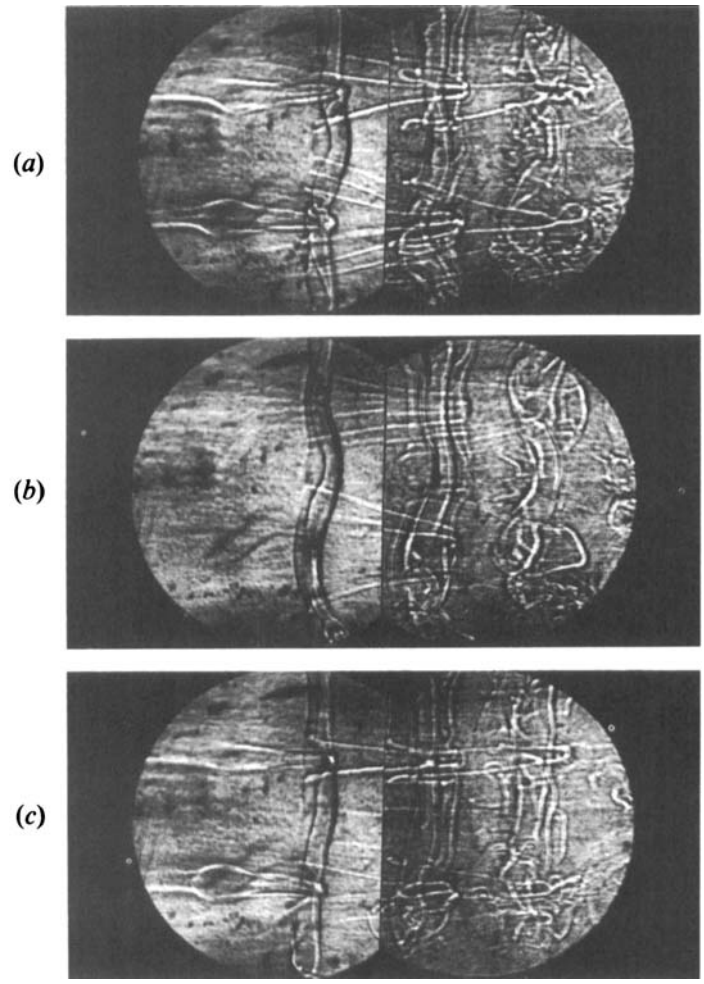

FIGURE 16. Composite schlieren plan (x, z) views showing the effect of phase distortions on the secondary vortices ($\lambda_z = 5.1$ cm, $\nu = 5$ Hz): (*a*) spanwise-periodic amplitude distribution E_{SP}, (*b*) $\Phi_{SP} = \Phi'(z)$ leading to the same deformations of the primary vortices as in (*a*); (*c*) excitation with E_{SP} and $\Phi_{SP} = -\Phi'(z)$.

In this section, it is shown that spanwise deformations of the primary vortices resulting from the appearance of secondary vortices can be suppressed (or cancelled) by external phase excitation. Furthermore, the suppression of the deformations of the primary vortices has a significant effect on the evolution of the secondary vortices. A time-harmonic excitation waveform having spanwise-uniform amplitude and frequency distributions is used along with video-imaging to determine a spanwise-periodic phase distribution $\Phi'(z)$ that leads to the same distortions of the primary vortices as in figure 16(*a*). The effect of phase excitation with $\Phi'(z)$ is shown in figure 16(*b*). While the core deformations of the primary vortices in figures 16(*a*) and 16(*b*) are reasonably similar, the secondary vortices in figure 16(*b*) are fully formed downstream of the first primary vortex on the left-hand side (and only partially rolled up upstream of that vortex). In common with figure 16(*a*) (and figure 5*h*, *i*), figure 16(*b*) also shows the formation of secondary vortex pairs on each side of the upstream bends of the primary vortices.

Figure 16(*c*) shows the response of the mixing layer to an excitation waveform

having spanwise-periodic amplitude distributions E_{SP} (as in figure 16*a*) and phase distribution $\Phi(z) = -\Phi'(z)$. The excitation is effected by a single row of surface heaters and is not a linear superposition of the excitation waveforms of figure 16(*a*, *b*). This is in contrast to the two-dimensional boundary-layer experiments of Liepmann, Brown & Nosenchuck (1982), where a linear disturbance excited by an upstream surface heater was cancelled by a phase-delayed input to a downstream surface heater. As a result of the modified (phase-corrected) excitation, the spanwise deformations of the primary vortices are almost completely suppressed, and the primary vortices remain almost undistorted throughout the streamwise domain shown in figure 16(*c*). As in figure 16(*a*), the secondary vortices are formed upstream of the first rollup of the primary vortices, where they appear to be unaffected by the spanwise phase of the excitation waveform. However, in the absence of the deformations of the primary vortices, the included angle Λ of the secondary vortex pairs remains almost unchanged with downstream distance compared to figure 16(*a*), and the additional secondary vortices that are present in figure 16 (*a*, *b*) are virtually absent. Furthermore, there is a noticeable diminution in small-scale motion within the core of the primary vortex at the downstream end of figure 16(*c*) compared to figure 16(*a*). This suggests that, in the absence of spanwise deformations, the cores of the primary vortices are more stable and that the onset of small-scale transition occurs farther downstream.

3.6. *Subharmonic phase excitation*

In the experiments described so far, phase excitation is effected at the fundamental (most-amplified) frequency of the shear layer and results in spanwise-non-uniform rollup and, consequently, in deformations of the primary vortices, with significant effects on their downstream evolution and on the formation of secondary vortices. Experimental observations (e.g. Keller *et al.* 1988; Delville *et al.* 1989) suggest that even far downstream from the domain of the initial rollup, the primary vortices continue to undergo complex spanwise deformations. These deformations apparently result from spanwise-non-uniform pairing interactions which, in the unforced shear layer, have been associated with the amplification of instability waves at subharmonics of the fundamental frequency. In this section it is demonstrated that spanwise-non-uniform pairings can be forced by a subharmonic wavetrain having spanwise-non-uniform phase or amplitude distributions.

To this end, the flow is excited by a linear superposition of a spanwise-uniform wavetrain at the fundamental frequency and a subharmonic wavetrain having spanwise-periodic and piecewise-constant amplitude (figure 17*a*) or phase (figure 17*b*) programmes. The respective amplitude and phase distributions of the subharmonic wavetrains in figure 17(*a*, *b*) have the same spanwise wavelength $\lambda_z = 20.3$ cm with a discontinuity at midspan. The fundamental excitation wavetrain results in a nominally spanwise-uniform rollup of the primary vortices while the lower streamwise amplification rate of the subharmonic wavetrain leads to pairings of the primary vortices farther downstream. As shown in figure 17(*a*, *b*), spanwise non-uniformities in either the amplitude or phase distributions of the subharmonic wavetrain can result in spanwise-non-uniform pairings. In the present experiments, the free-stream velocities are increased to 42 and 14 cm^{-1} so that the fundamental frequency is 9 Hz and $\lambda_{KH} = 3.1$ cm (for the subharmonic wavetrain, $\lambda_{KH-sh} = 6.2$ cm).

In figure 17(*a*), the phase of the subharmonic wavetrain is spanwise-invariant, and its amplitude distribution E_{Sp-sh} is $E_{0sh}(z) = 1.0E_0$ for $z < 0$ (i.e. below midspan in the x, z-view) and $E_{0sh}(z) = 0.3E_0$ for $z > 0$ (E_0 is the amplitude of the fundamental wavetrain). The higher amplitude of the subharmonic wavetrain for $z < 0$ leads to the

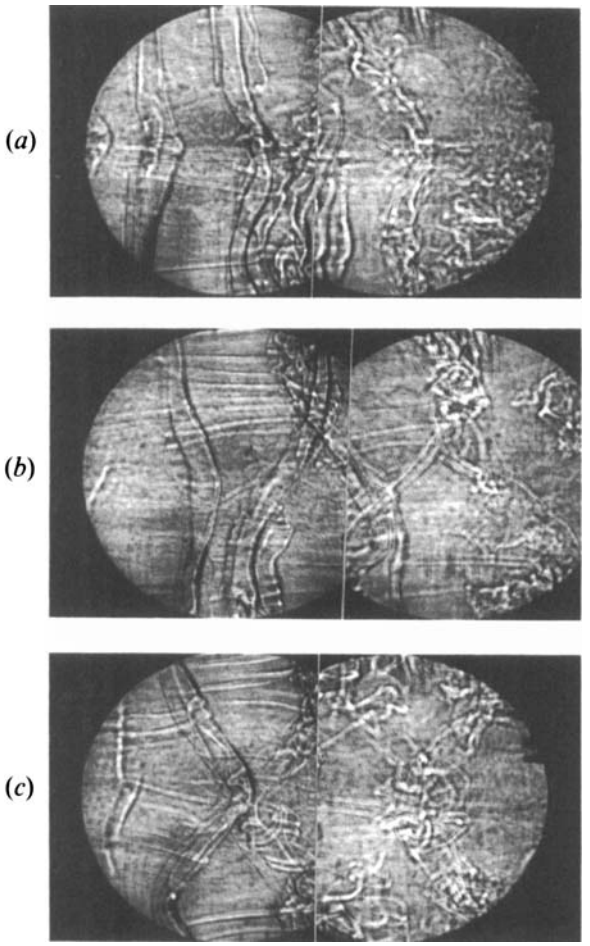

FIGURE 17. Composite schlieren plan (x, z) views where the excitation wavetrain is a linear combination of a spanwise-uniform fundamental and a spanwise-periodic subharmonic (sh); (a) E_{SP-sh} with $\lambda_z = 20.3$ cm ($E_{0sh} = E_0$ for $z < 0$ and $E_{0sh} = 0.3E_0$ for $z > 0$); (b) Φ_{SP-sh} with $\Delta\Phi = \pi$ and $\lambda_z = 20.3$ cm, and (c) Φ_{SP-sh} with $\Delta\Phi = \pi$ and $\lambda_z = 10.2$ cm. The free-stream velocities are 42 and 14 cm s^{-1} and $\nu = 9$ Hz.

occurrence of pairings of the primary vortices below midspan farther upstream than above midspan. The non-uniform pairing results in spanwise core deformations of the primary vortices and a substantial increase in small-scale motions within their cores at the downstream end of the schlieren view. After the pairings below and above midspan are completed, the (paired) spanwise vortices are branched about midspan in a manner reminiscent of figure 15(c). In figure 17(a), however, the streamwise distance between two connected segments of paired primary vortices below and above midspan depends on the magnitude of $E_{0sh}(z)$ (assuming that the streamwise amplification rate of the subharmonic wavetrain does not vary across the span).

In figure 17(b), the phase programme of the subharmonic wavetrain is Φ_{SP-sh} with $\Delta\Phi = \pi$ (relative to the segment $z > 0$) and its amplitude is spanwise-invariant (i.e. the subharmonic wavetrain is a linear superposition of pairs of equal and opposite oblique waves. Assuming that the streamwise amplification rates of adjacent segments of the subharmonic wavetrain are the same, then pairing of the spanwise vortices above and below midspan begins at approximately the same distance downstream of the flow

partition. Because of the phase change across midspan, the pairings alternate above and below $z = 0$ every half-period of the subharmonic wavetrain. These pairing interactions are similar to Pierrehumbert & Widnall's (1982) subharmonic instability, as demonstrated in figure 17(*c*) where the spanwise wavelength of the subharmonic wavetrain is reduced to 10.2 cm and phase discontinuities occur at $z = 5.1$, 0, and -5.1 cm. Figure 17(*c*) shows two pairing interactions centred at midspan and λ_{KH-sh} apart, and two other pairing interactions, each centred at $z = \pm 5.1$ cm (near the top and bottom edges of the schlieren view) and offset by $\frac{1}{2}\lambda_{KH-sh}$ in the streamwise direction relative to the pairing interactions at midspan. Of particular note is the increase in small-scale motion at the spanwise locations of the pairing interactions.

The photographs in figure 17(*a–c*) demonstrate that spanwise-non-uniform pairing and core deformations of the primary vortices far downstream from the flow partition of an unforced plane mixing layer can result from spanwise non-uniformities of amplitude and phase of subharmonic disturbances. This may explain the wide variety of spanwise-non-uniform pairing interactions that are apparent in plane mixing layers in the absence of deliberate excitation (e.g. Chandrsuda *et al.* 1978; Browand & Troutt 1980, 1985 and Keller *et al.* 1988).

4. Concluding remarks

The present investigation is concerned with the receptivity of the plane shear layer to perturbations resulting from spanwise phase variations of the fundamental and subharmonic instability modes of the nominally two-dimensional base flow. Phase perturbations are excited using time-harmonic wavetrains having spanwise-non-uniform phase or frequency distributions. Near the flow partition, phase distortions of an excitation wavetrain at the fundamental frequency result in spanwise-non-uniform rollup and core deformations of the primary vortices that persist throughout the present domain of observation. It appears that phase distortions and deformations of the base flow can continue to recur farther downstream through spanwise-non-uniform subharmonic (pairing) interactions of the primary vortices. An important consequence of the deformations of the primary vortices is the formation of secondary vortical structures in the braid region where their orientation and strength depend on the shape and degree of the deformation of the primary vortices.

Excitation with a spanwise-linear phase distribution (i.e. an oblique wavetrain) leads to the rollup of oblique primary vortices that are advected in the streamwise direction. The angles between the oblique vortices and the streamwise direction are virtually identical to the corresponding wave angles of the excitation wavetrain and remain almost invariant throughout the streamwise domain of observation ($X \leqslant 5.45$). The rollup of the primary vortices occurs along lines of constant phase of the excitation wavetrain and progresses obliquely as each vortex is advected downstream. Because the onset of oblique rollup for $\beta < 0.93\ \text{cm}^{-1}$ occurs at approximately the same streamwise location, it is concluded that the streamwise amplification of oblique waves for which $\psi < 30°$ is approximately the same. The streamwise inclination of the primary vortices is accompanied by a change in the direction of the principal strain in the braid region between them and, as a result, secondary vortices that are triggered by discretization discontinuities in the phase of the excitation waveform are approximately aligned with the wave vector of the excitation wavetrain.

Spanwise-periodic core deformations of the primary vortices are excited when the phase distribution of the excitation wavetrain is piecewise-constant (with a phase discontinuity $\Delta\Phi$) and spanwise-periodic (with wavelength λ_z). The excitation

waveform is a linear superposition of a two-dimensional time-harmonic wavetrain and a series of pairs of equal and opposite oblique wavetrains having wavenumbers that increase like n and amplitudes that decrease like $1/n$ ($n = 1, 2, \ldots$). The amplitudes of the two-dimensional and oblique wavetrains also vary with $\Delta\Phi$ such that when $\Delta\Phi = 0$ and π the oblique and two-dimensional wavetrains vanish, respectively. For any linear combination of two-dimensional and oblique excitation wavetrains there is a short-wavelength cutoff λ_{co} below which the primary vortices are not receptive to the excitation input. In particular, when $\Delta\Phi = \pi$, the primary vortices become unstable when the excitation wavelength exceeds λ_{KH}, or the spanwise wavenumber is below $\beta = 4\pi\nu/(U_1 + U_2)$. That the cutoff wavelength scales with λ_{KH} implies that λ_{co} increases with downstream distance and that phase disturbances of a given spanwise wavelength gradually decay as they are advected downstream.

Distortions of the primary vortices that result from phase variations of the excitation waveform are accompanied by the formation of secondary vortex strands. The evolution of these vortex strands depends critically on the magnitude of the spanwise phase variation and its characteristic spanwise wavelength. When the spanwise phase variation is small, the secondary vortices are counter-rotating vortex pairs that resemble the lambda studied by Lasheras & Choi (1988) and by N&G. However, as the phase variations increase, cross-shear induced by oblique segments of the primary vortices in the braid region results in the formation of single clockwise or counterclockwise secondary vortex strands that lack the symmetry of lambda vortices, and their strength increases with the phase variations. These vortex strands branch or bifurcate off the primary vortices and when the strength of the secondary vortices is comparable to that of the primary vortices ($\Delta\Phi \approx \pi$), the bifurcations appear to be unstable and continue along the axes of the primary vortices.

When the phase distribution is piecewise-constant and spanwise-periodic (Φ_{SP}) and $\Delta\Phi < \pi$ (or $> \pi$) (e.g. figure 5), lambda-shaped vortices are formed through the merging of adjacent counter-rotating pairs of secondary vortex strands each induced by a phase discontinuity of the excitation wavetrain. The strength and streamwise inclination of each leg of the secondary vortices increase with $\Delta\Phi$ (and with the deformations of the primary vortices). When $\Delta\Phi = \pi$, the deformed spanwise vortices resemble a pattern of diamond-shaped cells in the plane (x, z) view and may undergo localized pairings at streamwise edges of the diamond-shaped cells accompanied by a substantial increase in the momentum thickness. Although these vortical structures are reminiscent of the subharmonic pairing mode identified by Pierrehumbert & Widnall (1982), the streamwise wavelength in the present experiments is equal to the wavelength of the two-dimensional base flow. In fact, the spanwise-undulated primary vortices are formed at twice the excitation frequency through a double rollup and spanwise spreading of bifurcations of the primary vortices that are induced by spanwise phase discontinuities of the excitation waveform. In common with the subharmonic instability of Pierrehumbert & Widnall, the present results show the existence of a short-wavelength cutoff for excitation with pairs of equal and opposite oblique waves.

Similar to spanwise-non-uniform amplitude excitation, spanwise-non-uniform phase excitation can lead to significant spanwise and cross-stream distortion of time-averaged profiles of the streamwise velocity. The appearance of higher-order inflectional instabilities, where broadband perturbations already present in the base flow are amplified, results in spanwise-non-uniform concentrations of small-scale motion. Power spectra of the streamwise velocity component show that the width of the mixing layer increases substantially when $\Delta\Phi = \pi$, as indicated by cross-stream spreading of high-frequency spectral components associated with small-scale motion.

When streamwise counter-rotating vortex pairs are deliberately triggered upstream of the rollup of the spanwise vortices, core deformations of the latter play an important role in the subsequent generation of small-scale motion. This was demonstrated by suppression of core deformation via appropriate modification of the phase distribution of the excitation wavetrain. While the modified excitation wavetrain does not affect the formation of the secondary vortices, in the absence of core deformations the secondary vortices appear to be weaker and have smaller included angles that are almost invariant with downstream distance. These changes are accompanied by a reduction in small-scale motions within the cores of the primary vortices, indicating that, in the absence of core deformations, small-scale transition begins farther downstream.

Experimental evidence (e.g. Browand & Ho 1987; Keller *et al.* 1988; Delville *et al.* 1989) suggest that phase distortions of the base flow can also occur far downstream of the flow partition and, given their characteristic spanwise wavelength, it appears that they are connected with the amplification of subharmonic modes. Thus, it is conjectured that far downstream of the flow partition, the excitation is effected through the amplification of a hierarchy of fundamental and subharmonic instability modes of the two-dimensional base flow where the subharmonic disturbances could be present either in the flow partition's boundary layer or in one or both of the free streams. Consecutive subharmonic modes having streamwise wavelengths $\lambda_{sh} = n\lambda_{KH}$ (where λ_{KH} is the wavelength of the fundamental instability and $n = 2, 3, \ldots$) amplify, become neutral and finally decay within corresponding finite and partially overlapping streamwise domains that extend downstream of the flow partition (Ho & Huerre 1984). Near the flow partition, phase distortions of the fundamental wavetrain result in spanwise-non-uniform rollup and thus in core deformations of the primary vortices that persist throughout the present domain of observation ($X \leqslant 5.45$).

To demonstrate that phase deformations of the nominally two-dimensional base flow can recur far downstream from the flow partition through subharmonic (pairing) interactions, the flow is excited with a linear superposition of two time-harmonic excitation wavetrains, one at the fundamental frequency and the other at the first subharmonic. The fundamental wavetrain is spanwise uniform, while the subharmonic has a spanwise-periodic and piecewise-constant amplitude or phase distribution. The two-dimensional excitation results in a nominally spanwise-uniform rollup of the primary vortices while the lower streamwise amplification rate of the subharmonic wavetrain leads to spanwise-non-uniform pairings farther downstream. The paired spanwise vortices become branched and spanwise-undulated much like the evolution of the spanwise vortices in the far field of unforced shear layers. When the subharmonic wavetrains have a spanwise-periodic phase distribution with $\Delta\Phi = \pi$, the pairing interactions are essentially the same as Pierrehumbert & Widnall's (1982) subharmonic instability.

That the appearance of the secondary vortices (and regions of cross-shear) in the braids region results in a substantial increase in small-scale motions within the cores of the primary vortices suggests that core deformations and spanwise-non-uniform pairings of the primary vortices may be critical to the continuation of small-scale mixing downstream from the mixing transition of an unforced plane shear layer. This also suggests that phase excitation may enable the control of mixing downstream of mixing transition by exploiting spanwise phase and amplitude non-uniformities of disturbances at subharmonics of the fundamental frequency.

The authors wish to acknowledge a number of valuable discussions with Professors F. K. Browand and W. C. Reynolds and Drs R. D. Moser and M. M. Rogers. This

work has been supported by AFOSR Grants 86-0324 and 88-0271 monitored by Dr J. M. McMichael. Partial support was also provided by NSF Engineering Research Initiation Grant MSM-8505234 and through the NASA Graduate Student Researchers Program (Grant NGT-50076).

REFERENCES

ASHURST, W. T. & MEIBURG, E. 1988 Three-dimensional shear layers via vortex dynamics. *J. Fluid Mech.* **189**, 87–116.

ATSAVAPRANEE, P. & GHARIB M. 1994 A study of a plane mixing layer with cross shear. *Phys. Fluids* (in press).

BREIDENTHAL, R. E. 1981 Structure in turbulent mixing layers and wakes using a chemical reaction. *J. Fluid Mech.* **109**, 1–24.

BROWAND, F. K. & HO, C.-M. 1987 Forced unbounded shear flows. *Nuclear Phys.* B **2**, 139–158.

BROWAND, F. K. & PROST-DOMASKY, S. 1990 Experiment on pattern evolution in the two-dimensional mixing layer. In *New Trends in Nonlinear Dynamics and Patterning Phenomena: The Geometry of Non-Equilibrium* (ed. P. Coullet & P. Huerre). NATO ASI Series 8, pp. 159–170. Plenum.

BROWAND, F. K. & TROUTT, T. R. 1980 A note on spanwise structure in the two-dimensional mixing layer. *J. Fluid Mech.* **97**, 771–781.

BROWAND, F. K. & TROUTT, T. R. 1985 The turbulent mixing layer: geometry of large vortices. *J. Fluid Mech.* **158**, 489–509.

CHANDRSUDA, C., MEHTA, R. D., WEIR, A. D. & BRADSHAW, P. 1978 Effect of free-stream turbulence on large structures in turbulent mixing layers. *J. Fluid Mech.* **85**, 693–704.

COLLIS, S. S., LELE, S. K., MOSER, R. D. & ROGERS, M. M. 1991 Time developing mixing layer with spanwise-nonuniform phase. *Bull. Am. Phys. Soc.* **36**, 2660.

COLLIS, S. S., LELE, S. K., MOSER, R. D. & ROGERS, M. M. 1994 The evolution of a plane mixing layer with spanwise nonuniform forcing *Phys. Fluids* **6**, 381–396.

COMTE, P. & LESIEUR, M. 1991 Large- and small-scale stirring of vorticity and a passive scalar in a 3D temporal mixing layer. *Phys. Fluids* A **3**, 1451.

CORCOS, G. M. & LIN, S. J. 1984 The mixing layer: deterministic models of a turbulent flow. Part 2. The origin of the three-dimensional motion. *J. Fluid Mech.* **139**, 67–95.

DALLARD, T. & BROWAND, F. K. 1993 The growth of large scales at defect sites in the plane mixing layer. *J. Fluid Mech.* **247**, 339–368.

DELVILLE, J., BELLIN, S., GAREM, J. H. & BONNET, J. P. 1989 Analysis of structures in a turbulent plane mixing layer by use of pseudo flow visualization method based on hot wire anemometry. In *Advances in Turbulence 2* (ed. H.-H. Fernholtz & H. E. Fiedler). Springer.

GLEZER, A., KATZ, Y. & WYGNANSKI, I. 1989 On the breakdown of a wave packet trailing a turbulent spot in a laminar boundary layer. *J. Fluid Mech.* **198**, 1–26.

HAMA, F. R., RIST, U., KONZELMAN, U., LAURIEN, E. & MEYER, F. 1987 Vorticity field structure associated with 3D Tollmien–Schlichting waves. *Sādhanā* **10**, 321–347.

HO, C.-M. & HUERRE, P. 1984 Perturbed free shear layers. *Ann. Rev. Fluid Mech.* **16**, 365–424.

KELLER, J. O., ELLZEY, J. L., PITZ, R. W., SHEPHARD, I. G. & DAILY, J. W. 1988 The structure and dynamics of reacting plane mixing layers. *Exp. Fluids* **6**, 33–43.

LASHERAS, J. C., CHO, J. S. & MAXWORTHY, T. 1986 On the origin and evolution of streamwise vortical structures in a plane, free shear layer. *J. Fluid Mech.* **172**, 231–258.

LASHERAS, J. C. & CHOI, H. 1988 Three-dimensional instability of a plane free shear layer: an experimental study of the formation and evolution of streamwise vortices. *J. Fluid Mech.* **189**, 53–86.

LASHERAS, J. C. & MEIBURG, E. 1990 Three-dimensional vorticity modes in the wake of a flat plate. *Phys. Fluids* A **3**, 371–379.

LIEPMANN, H. W., BROWN, G. L. & NOSENCHUCK, D. M. 1982 Control of laminar instability-waves using a new technique. *J. Fluid Mech.* **118**, 187–200.

MEIBURG, E. & LASHERAS, J. C. 1988 Experimental and numerical investigation of the three-dimensional transition in a plane wakes. *J. Fluid Mech.* **190**, 1–37.

NASSEF, H. & BROWAND, F. K. 1993 On the formation of a defect structure in a two-dimensional mixing layer. *Phys. Fluids* A **5**, 979–983.

NYGAARD, K. J. 1991 Spanwise-nonuniform excitation of a plane mixing layer. PhD thesis, University of Arizona.

NYGAARD, K. J. & GLEZER, A. 1990 Core instability of the spanwise vortices in a plane mixing layer. *Phys. Fluids* A **2**, 461–464.

NYGAARD, K. J. & GLEZER, A. 1991 Evolution of streamwise vortices and the generation of small-scale motion in a plane mixing layer. *J. Fluid Mech.* **231**, 257–301 (referred to herein as N&G).

PIERREHUMBERT, R. T. & WIDNALL, S. E. 1982 The two- and three-dimensional instabilities of a spatially periodic shear layer. *J. Fluid Mech.* **114**, 59–82.

ROBEY, H. F. 1987 The nature of oblique instability waves in boundary layer transition. In *Turbulence Management and Relaminarization, Proc. IUTAM Symp, Bangalore, India* (ed. H. W. Liepmann & R. Narasima), pp. 187–198. Springer.

ROOS, F. W., KEGELMAN, J. T. & KIBENS, V. 1989 Two stream mixing layer from a swept trailing edge. *AIAA Paper* 89–1022.

SANDHAM, N. D. & REYNOLDS, W. C. 1991 Three-dimensional simulations of large eddies in the compressible mixing layer. *J. Fluid Mech.* **224**, 133–158.

SCHNEIDER, S. P. 1989 Effects of controlled three-dimensional perturbations on boundary layer transition. PhD thesis, California Institute of Technology.

WILLIAMSON, C. H. K. 1989 Generation of periodic dislocations due to a point disturbance in a planar wake. *Phys. Fluids* A **1**, 1444.

WILLIAMSON, C. H. K. 1992 The natural and forced formation of spot-like 'vortex dislocations' in the transition of a wake. *J. Fluid Mech.* **243**, 393–441.

WILLIAMS-STUBER, K. & GHARIB, M. B. 1989 Study of the origin of three-dimensional structures and chaos in an externally forced free shear layer. *AIAA Paper* 89-1021, *2nd Shear Flow Conf., March 13–16, Tempe, Arizona.*